AD_____
(Leave blank)

Award Number: W81XWH-09-1-0180

TITLE: Development of Novel Treatment Plan Verification Techniques for Prostate Intensity Modulation Arc Therapy

PRINCIPAL INVESTIGATOR: Wu Liu, Ph.D.

CONTRACTING ORGANIZATION: Stanford University
Stanford, CA 94305

REPORT DATE: March 2010

TYPE OF REPORT: Annual Summary

PREPARED FOR: U.S. Army Medical Research and Materiel Command
Fort Detrick, Maryland 21702-5012

DISTRIBUTION STATEMENT: (Check one)

☒ Approved for public release; distribution unlimited

☐ Distribution limited to U.S. Government agencies only; report contains proprietary information

The views, opinions and/or findings contained in this report are those of the author(s) and should not be construed as an official Department of the Army position, policy or decision unless so designated by other documentation.

REPORT DOCUMENTATION PAGE

Form Approved
OMB No. 0704-0188

1. REPORT DATE *(DD-MM-YYYY)*	2. REPORT TYPE	3. DATES COVERED *(From - To)*
01-03-2010	Annual Summary	1 Mar 2009 - 28 Feb 2010

4. TITLE AND SUBTITLE

Development of Novel Treatment Plan Verification Techniques for Prostate Intensity Modulation Arc Therapy

5a. CONTRACT NUMBER

5b. GRANT NUMBER
W81XWH-09-1-0180

5c. PROGRAM ELEMENT NUMBER

6. AUTHOR(S)

Liu, Wu

Email: wuliu@stanford.edu

5d. PROJECT NUMBER

5e. TASK NUMBER

5f. WORK UNIT NUMBER

7. PERFORMING ORGANIZATION NAME(S) AND ADDRESS(ES)

Stanford University,
Stanford, CA 94305

8. PERFORMING ORGANIZATION REPORT NUMBER

9. SPONSORING / MONITORING AGENCY NAME(S) AND ADDRESS(ES)

10. SPONSOR/MONITOR'S ACRONYM(S)

11. SPONSOR/MONITOR'S REPORT NUMBER(S)

12. DISTRIBUTION / AVAILABILITY STATEMENT

Approved for public release; distribution unlimited

13. SUPPLEMENTARY NOTES

14. ABSTRACT

For fractionated treatment, adaptive radiation therapy (ART) is a strategy of which the subsequent fractional delivery can be adaptively modified based on a closed-loop control framework using systematic feedback of geometric and dosimetric information. However, a critical component that is missing in current linac-based radiation therapy is a treatment plan verification system capable of validating and documenting the dose delivered and preventing geographic misses, especially for modern volumetric intensity modulated arc therapy (VMAT). The objective of this project is to develop a novel clinical useful delivered-dose verification protocol for modern prostate VMAT using Electronic Portal Imaging Device (EPID) and onboard Cone beam Computed Tomography (CBCT). We have carried a systematic study on developing the CBCT and EPID imaging based dose verification technique. A number of important milestones have been accomplished, which include (i) calibrated CBCT HU vs. electron density curve; (ii) established technical infrastructures for deformable registration between CBCT and pCT and detecting MLC leaf end positions using EPID images acquired during treatment; (iii) developed a gantry and imager geometric calibration procedure; (iv) developed an intrafraction prostate motion monitoring and correction strategy and a dose reconstruction technique for treatment plan verification; and (v) performed phantom studies using the developed techniques.

15. SUBJECT TERMS

prostate cancer, dose verification, intrafraction motion, image guided radiation therapy

16. SECURITY CLASSIFICATION OF:			17. LIMITATION OF ABSTRACT	18. NUMBER OF PAGES	19a. NAME OF RESPONSIBLE PERSON
a. REPORT	b. ABSTRACT	c. THIS PAGE			USAMRMC
U	U	U	UU	33	19b. TELEPHONE NUMBER *(include area code)*

Table of Contents

Page

I. Introduction

This Postdoctoral Training Award (W81XWH-09-1-0180, entitled "Development of Novel Treatment Plan Verification Techniques for Prostate Intensity Modulation Arc Therapy") was awarded to the principal investigator (PI), Wu Liu, for the period of March 1, 2009 – February 28, 2011. This is the annual report for the first funding period (March 1, 2009 – February 28, 2010).

Radiation therapy of prostate cancer is the subject of this project. For fractionated treatment, adaptive radiation therapy (ART) is a strategy of which the subsequent fractional delivery can be adaptively modified based on a closed-loop control framework using systematic feedback of geometric and dosimetric information. However, a critical component that is missing in current linac-based radiation therapy is a treatment plan verification system capable of validating and documenting the dose delivered and preventing geographic misses, especially for modern intensity volumetric modulated arc therapy (VMAT). The objective of this project is to develop a novel clinical useful delivered-dose verification protocol for modern prostate VMAT using Electronic Portal Imaging Device (EPID) and onboard Cone beam Computed Tomography (CBCT). The specific aims of this project are: (i) to calibrate the CBCT and to establish an accurate deformable registration framework for registration of the prostate CBCT images to the planning CT images; (ii) to develop and evaluate a method of measuring the leaf end position during delivery by EPID and re-constituting the multi-leaf collimator (MLC) leaf sequence (LS); (iii) to incorporate geometric corrections of the gantry and imager; (iv) to evaluate the achievable accuracy in using a CBCT and measured LS, therefore, fluence map for dose calculation.

Under the generous support from the U.S. Army Medical Research and Materiel Command (USAMRMC), the PI has contributed significantly to the field of prostate cancer research by applying advanced physics and computer vision knowledge. A number of conference abstracts and peer-reviewed journal publications have been resulted from the support. In this report, the PI's research activities in the first funding year are highlighted.

II. Body

The PI has gradually started working on the proposed work since the proposal was submitted. Task 1 is to calibrate the CBCT, to establish an accurate deformable registration framework for registration of the prostate CBCT images to the pCT images. This step is to build a technical infrastructure for the ultimate goal of dose verification. It has been completed as described below.

It is necessary to relate the HU of the scanner with the actual electron density in order to use planning CT (pCT) or CBCT for radiation dose calculation. A CT-phantom, Catphan-600 module CTP404, was used for the calibration of pCT and CBCT. The HU differences between the measured results of pCT and CBCT were less than 10 HU for the 8 objects with known electron density in the phantom and CT number ranging from -1000 HU (air) to 930 (Telfon). The calibration was repeated 10 times over 3 months for CBCT. No significant variations were found. The results show that it is valid to use CBCT HU for dose reconstruction.

Due to the rectal filling changes between the days that pCT and CBCT were acquired, the intensity-based deformable registration had severely problem to accurately mapping the contours on the pCT to CBCT. Therefore, a feature-based narrow band deformable registration algorithm is used and satisfactory results were found. The method first searches control points using scale invariance feature transformation (SIFT) in a narrow band (1 – 1.5 cm wide ring) outside the rectal wall to avoid the rectal filling problem. It then performs a thin plate spline transformation to warp the narrow band and mapping the corresponding contours from pCT to CBCT. Further test for this selected algorithm used in dose reconstruction will be performed at the evaluation phase of proposed technique (task 4).

Task 2 is to develop and evaluate a method of measuring the leaf end position during delivery by EPID and re-constituting the multi-leaf collimator. This step is to develop a way to extract useful MLC leaf position information from EPID images for later dose reconstruction, and to design a method utilizing the EPID images to compensate for the adverse effect of intrafraction prostate motion for more accurate dose delivery, therefore verify the delivered dose is reasonably close to the planned dose. It has almost been completed as described below.

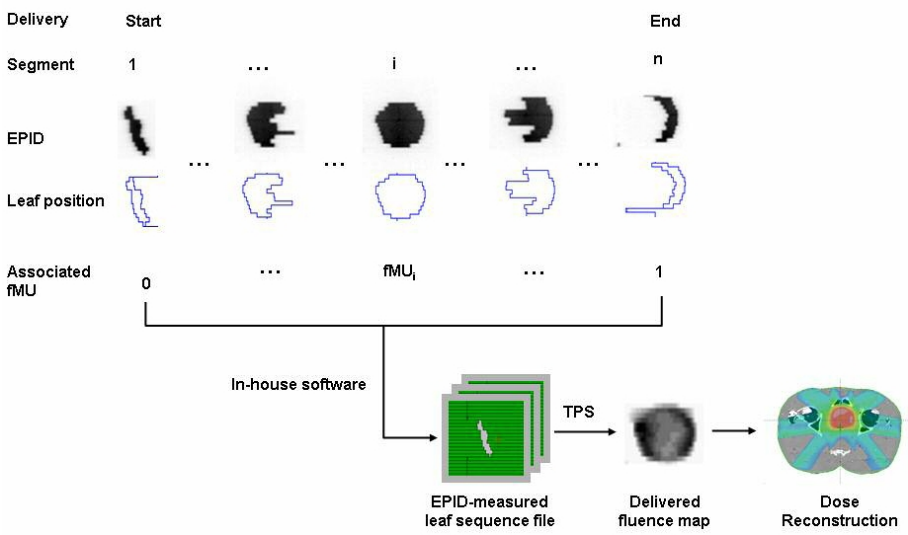

Fig. 1. Workflow of leaf sequence re-constitution.

Because of the high contrast between the irradiated and non-irradiated area on the EPID MV images, it is relatively easy to detect the MLC leaf ends using edge detectors that are not very complicated. We search the positions of the leaf ends near the penumbral regions by a maximum gradient edge detection algorithm in a scan line fashion for the pixels rows. The maximum gradient in intensity in the penumbral region was considered as the leaf end position ($\vec{U}$). The pixel location is spatially converted and projected back to the isocentric plane. The leaf positions on isocentric plane ($\vec{X}$) in a perfect imaging geometry is $\vec{X} = \vec{U} \cdot SAD/SID$, where SAD is the source-to-axis distance and SID is the source-to-imager distance. A MLC leaf sequence (LS) file is reconstituted (Fig. 1) using the EPID-measured segmental leaf positions and their associated fractional MUs by matching the gantry information from EPID images and the machine's delivery log files. The LS file will be used later for the

delivered dose reconstruction. One problem we are currently encountering is that cine EPID imaging during VMAT delivery is not recommended for our current Varian linac machine because of a high dose rate issue. Therefore, our leaf position detection experiments are conducted using conformal arc delivery. The new generation Varian machine, which will be installed in our clinic in a couple of months, however, provides the ability to take cine EPID during VMAT delivery. The detection procedure is expected to be exactly the same.

A necessary step in combating the adverse dosimetric effects of intrafraction prostate motion is the real-time monitoring of the target position. All existing motion tracking techniques seek to accurately and continuously localize the prostate target. Fluoroscopic imaging with one or two kV sources poses the problem of accumulating excessive patient imaging dose. Because intrafraction prostate motion is generally unpredictable, we developed a novel coarse-to-fine two-step failure detection-based motion tracking technique that effectively uses cine-MV data to provide a clinically valuable way to minimize kV usage, while maintaining high targeting accuracy. This method minimizes the difference between actual delivered and planned dose to prostate patients. The simulation results were presented at the 2009 annual conference of the American Association of Physicists in Medicine (AAPM) [1] and has been accepted to publish in the International Journal of Radiation Oncology, Biology, Physics [2].

Task 3 is to incorporate geometric corrections of the gantry and imager. This step is to compensate for the geometric errors at different gantry angles so that we can use more accurate MLC leaf positions to reconstitute LS-files and therefore more accurately reconstruct the delivered dose. This step has been completed as described below.

A robust procedure of system calibration for the MV EPID and on-board kV imager is developed for patient imaging during intensity modulated arc delivery. The results were published in the journal Physics in Medicine and Biology [3]. The calibration procedure helps to correct the geometric errors caused by gantry sag and imager tilt. The online real-time imaging spatial accuracy was significantly improved to better than 0.5 mm for all gantry positions during arc delivery. Therefore, it is made possible for image-based dose reconstruction of delivered dose to the patient. After geometric correction, the mean deviation of the EPID-measured leaf positions from the planned leaf positions is about 0.6 – 1.0mm. It means that the actual delivered dose would be different from the planned dose. This is one of the major reasons why we need this technique to verify the delivered dose and for future development of adaptive radiation therapy to compensate for the dose discrepancy.

Task 4 is to evaluate the achievable accuracy in using a CBCT and measured LS, therefore, fluence map for dose calculation. The step is to reconstruct the delivered dose using the information acquired during the treatment with the techniques developed in tasks 1 – 3. The major concern is that the intrafraction prostate motion changes the patient anatomy and deteriorates the dose delivery. We are developing method to minimize the effect from intrafraction prostate motion and improve the dose reconstruction accuracy and in progress of evaluating the proposed methods using phantom and patient data.

Because VMAT delivers the dose in an arc during gantry rotation, images are available from different viewing angles. Therefore, by taking the advantage of gantry rotation, the target position can be stereoscopically reconstructed using the MV images acquired at different gantry angle. In conjunction with applying our proposed failure detection-based motion tracking technique, we developed an optimized MV-kV motion monitoring strategy during intensity modulated arc therapy, which can be used to ensure and verify the treatment dose delivered to the patient is in accordance with the treatment plan. The simulation and experimental results were presented at the 2009 annual conference of the American Association of Physicists in Medicine (AAPM) [4], the 2009 annual conference of the American Society for Therapeutic Radiology and Oncology (ASTRO) [5] and has been accepted to publish in the International Journal of Radiation Oncology, Biology, Physics [6].

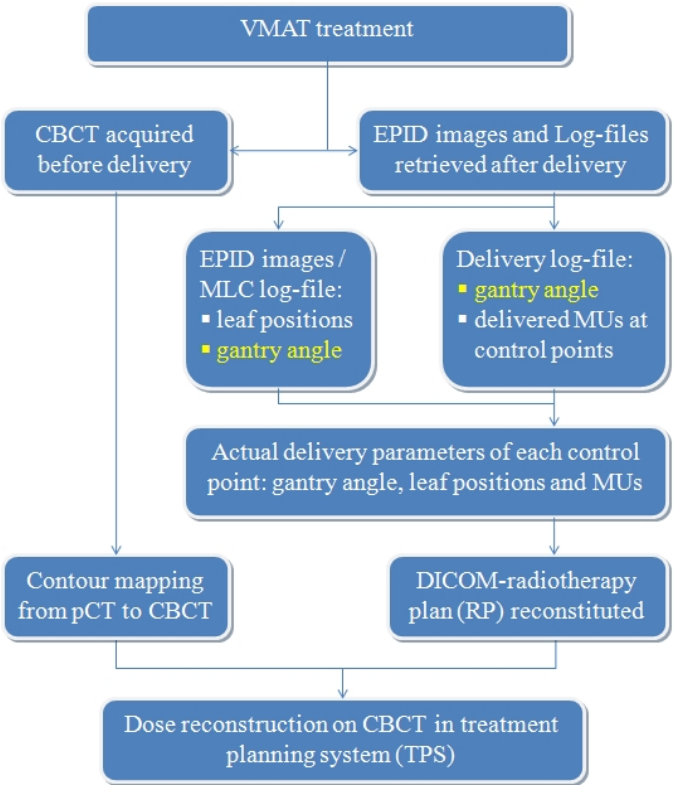

Fig. 2. Workflow of the VMAT dose reconstruction and plan verification procedure.

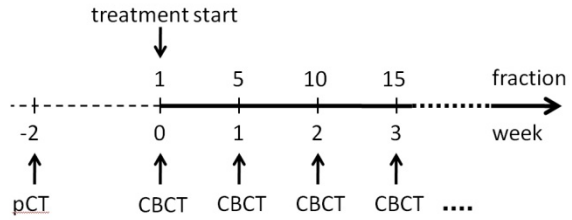

Fig. 3. Timeline showing the scheduling of planning CT and CBCT.

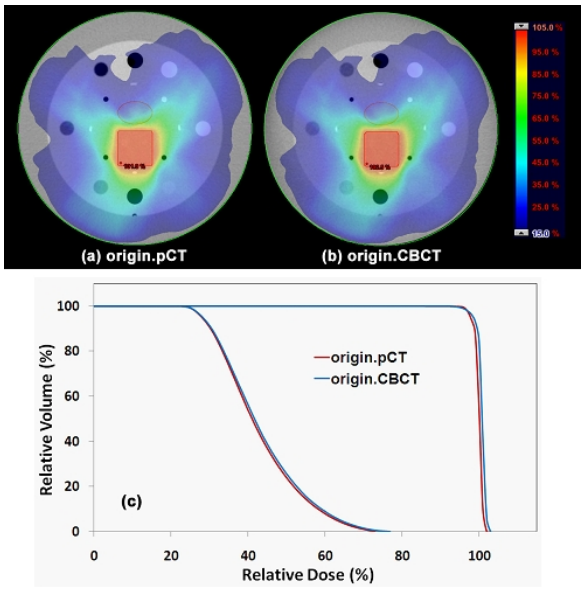

Fig. 4. Dose distributions of (a) the original plan on the planning CT and (b) the same plan on the CBCT. (c) DVHs of the target and organ at risk for the two calculations.

We established a methodology to reconstruct the delivered dose of a VMAT treatment using on-treatment CBCT and reconstituted DICOM-radiotherapy plan (RP) file based on EPID-measured MLC leaf positions or MLC dynamic log-files and delivery log-files containing the actual geometric and dosimetric information of the delivery. Figure 2 shows the workflow of the dose reconstruction and plan verification method. Figure 3 shows the CBCT and planning CT (pCT) scheduling. The Catphan-600

phantom study demonstrated the feasibility of using CBCT for dose calculation. CBCT was performed before the dose delivery. The systematic log-files were retrieved after the delivery and the leaf positions were measured and logged from EPID images during treatment. Actual delivery at a control point including MLC leaf positions, gantry angles and cumulative monitor units (MUs) were recorded in the log-files and the information was extracted using in-house developed software. The extracted information was then embedded into the original treatment DICOM-RP file to replace the original control point parameters. This reconstituted DICOM-RP file was imported into the Eclipse treatment planning system (TPS) and dose was computed on the corresponding CBCT. A series of phantom experiments was performed on a Varian Trilogy™ medical linear accelerator to show the feasibility of dose reconstruction, validate the procedure, and demonstrate the efficacy of this methodology. The resultant dose distributions and dose volume histograms (DVHs) were compared with that of the original treatment plan. For example, figure 4 shows that the CBCT-based dose distributions agree with that of the pCT-based original plan very well at the absence of target motion. The DVH in Figure 4 of the CBCT-based plan shows a dose increase of 0.8% for the entire target volume in comparison with the original pCT-based plan. The discrepancy in the dose maximum of the target is 1.3% and the discrepancy in the mean target dose is 0.7%. The studies indicated that CBCT-based VMAT dose reconstruction is readily achievable and provides a valuable tool for monitoring the dose actually delivered to the tumor target as well as the sensitive structures. In the absence of setup errors, the reconstructed dose shows no significant difference from the original planning CT-based plan. It is also elucidated that, the proposed method is capable of revealing the dosimetric changes in the presence of setup errors. This maneuver provides a valuable clinical tool for us to assure the VMAT dose delivery. The proposed dose reconstruction procedure is applicable in clinic and may find applications in the future adaptive VMAT with the actual delivered dose considered in the clinical decision-making process. The initial data analysis has been completed and the results are being submitted to the journal Physics in Medicine and Biology for consideration of publication.

III. Key Research Accomplishments

- Calibrated the CBCT for electron density vs. Hounsfield unit and compared the results for planning CT. It is validated that CBCT HU may be used for dose reconstruction.
- Selected and tested using SIFT features in a narrow band for thin plate spline deformable registration. The method gives clinically acceptable results.
- Selected and confirmed the feasibility of using maximum gradient edge detection algorithm for MLC leaf end position detection.
- Developed a novel prostate intrafraction motion monitoring and correction technique based the concept of failure detection. This method significantly reduced the unwanted kV imaging dose to patient, while maintaining high clinical targeting accuracy.
- Developed a system calibration procedure for the MV EPID and on-board kV imager used for patient imaging during VMAT.

- Developed a novel strategy for motion correction during VMAT and minimize the deviation of delivered patient dose from the planned dose by utilizing the proposed failure detection technique and taking the advantage of gantry rotation when dose is delivered in an arc.
- Established a novel methodology and procedure for retrospectively reconstructing the actual dose delivered in VMAT based on the pre-treatment (CBCT), EPID images and dynamic log-files during treatment has been established. It can be used to dosimetrically evaluate the delivery accuracy of the VMAT treatment plan. Phantom studies have been performed.

IV. Reportable Outcomes

The following is a list of publications resulted from the grant support in the last funding period.

Refereed Publications:

1. Liu, W., G. Luxton, and L. Xing, *A Failure Detection Strategy for Intrafraction Prostate Motion Monitoring with On-board Imagers for Fixed-Gantry IMRT.* International Journal of Radiation Oncology Biology Physics, 2010. In press.
2. Liu, W., R.D. Wiersma, and L. Xing, *Optimized Hybrid MV-kV Imaging Protocol for Volumetric Prostate Arc Therapy.* International Journal of Radiation Oncology Biology Physics, 2010. In press.

Conference Abstracts:

1. Liu, W., et al., *Intrafraction Prostate Motion Monitoring with Cine-MV and Minimal As-Needed Onboard KV Imaging.* Medical Physics, 2009. **36**: p. 2724. Presented at 2009 AAPM annual conference, July 2009, Anaheim, CA
2. Liu, W., et al., *Real-Time Motion Detection of Prostate Target During Volumetric Arc Therapy Using Onboard Imaging Devices.* Medical Physics, 2009. **36**: p. 2800-2801. Presented at 2009 AAPM annual conference, July 2009, Anaheim, CA
3. Liu, W., G. Luxton, and L. Xing, *Optimized Hybrid MV-kV Imaging Protocol for Volumetric Prostate Arc Therapy.* International Journal of Radiation Oncology Biology Physics, 2009. **75**(3): p. S570-S571. Presented at 2009 ASTRO annual conference, November 2009, Chicago, IL

V. Conclusion

In summary, an infrastructure has been established to execute the proposed research. System calibration procedures have been developed. Novel intrafraction prostate motion monitoring and correction strategy and dose reconstruction technique for treatment plan verification have been proposed for the radiation therapy treatment of prostate cancer. Phantom studies on reconstruction of actual delivered dose have been performed. A few milestones have been achieved toward the general goal of the project. Further improvement of the developed technique by refining deformable image registration between pCT and CBCT and evaluation of the proposed dose verification technique using real patient data are under study. This project paves the road of a critical translation of advanced physics research into clinical use for the benefits of prostate cancer patients.

VI. References

1. Liu, W., et al., *Intrafraction Prostate Motion Monitoring with Cine-MV and Minimal As-Needed Onboard KV Imaging.* Medical Physics, 2009. **36**: p. 2724.
2. Liu, W., G. Luxton, and L. Xing, *A Failure Detection Strategy for Intrafraction Prostate Motion Monitoring with On-board Imagers for Fixed-Gantry IMRT.* International Journal of Radiation Oncology Biology Physics, 2010. **to appear**.
3. Liu, W., et al., *Real-time 3D internal marker tracking during arc radiotherapy by the use of combined MV-kV imaging.* Physics in Medicine and Biology, 2008. **53**(24): p. 7197-7213.
4. Liu, W., et al., *Real-Time Motion Detection of Prostate Target During Volumetric Arc Therapy Using Onboard Imaging Devices.* Medical Physics, 2009. **36**: p. 2800-2801.
5. Liu, W., G. Luxton, and L. Xing, *Optimized Hybrid MV-kV Imaging Protocol for Volumetric Prostate Arc Therapy.* International Journal of Radiation Oncology Biology Physics, 2009. **75**(3): p. S570-S571.
6. Liu, W., R.D. Wiersma, and L. Xing, *Optimized Hybrid MV-kV Imaging Protocol for Volumetric Prostate Arc Therapy.* International Journal of Radiation Oncology Biology Physics, 2010. **to appear**.

VII. Appendices

Peer-reviewed publications in the last funding period.

Int. J. Radiation Oncology Biol. Phys., Vol. ■, No. ■, pp. 1–8, 2010

0360-3016/10/$–see front matter

ELSEVIER

doi:10.1016/j.ijrobp.2009.12.068

PHYSICS CONTRIBUTION

A FAILURE DETECTION STRATEGY FOR INTRAFRACTION PROSTATE MOTION MONITORING WITH ON-BOARD IMAGERS FOR FIXED-GANTRY IMRT

Wu Liu, Ph.D.,* Gary Luxton, Ph.D.,* and Lei Xing, Ph.D.*

From the *Department of Radiation Oncology, Stanford University School of Medicine, Stanford, CA

Purpose: To develop methods to monitor prostate intrafraction motion during fixed-gantry intensity-modulated radiotherapy using MV treatment beam imaging together with minimal kV imaging for a failure detection strategy that ensures prompt detection when target displacement exceeds a preset threshold.
Methods and Materials: Real-time two-dimensional (2D) marker position in the MV image plane was obtained by analyzing cine-MV images. The marker's in-line movement, and thus its time-varying three-dimensional (3D) position, was estimated by combining the 2D projection data with a previously established correlative relationship between the directional components of prostate motion. A confirmation request for more accurate localization using MV-kV triangulation was triggered when the estimated prostate displacement based on the cine-MV data was greater than 3 mm. An interventional action alert followed on positive MV-kV confirmation. To demonstrate the feasibility and accuracy of the proposed method, simulation studies of conventional-fraction intensity-modulated radiotherapy sessions were done using 536 Calypso-measured prostate trajectories from 17 radiotherapy patients.
Results: A technique for intrafraction prostate motion management has been developed. The technique, using "freely available" cine-MV images and minimum on-board kV imaging (on average 2.5 images/fraction), successfully limited 3D prostate movement to within a range of 3 mm relative to the MV beam for 99.4% of the total treatment time. On average, only approximately one intervention/fraction was needed to achieve this level of accuracy.
Conclusion: Instead of seeking to accurately and continuously localize the prostate target as existing motion tracking systems do, the present technique effectively uses cine-MV data to provide a clinically valuable way to minimize kV usage, while maintaining high targeting accuracy. © 2010 Elsevier Inc.

Intrafraction prostate motion, Onboard imaging, Motion tracking, Failure detection.

INTRODUCTION

A prostate motion management technique is critical for modern highly conformal and dose-escalated prostate radiation therapy. Conventional techniques used for prostate position monitoring include use of MV or kV images taken immediately before and after a treatment fraction (1), or, in some cases, before each field for intensity-modulated radiotherapy (IMRT) (2). Analysis of continuous real-time monitoring data suggests, however, that these methods do not sufficiently monitor prostate motion, because the prostate may undergo sudden displacements during intervals when imaging is not present (3, 4). Intrafraction prostate motion management is certainly desirable and has recently become an active research topic (4–8). Although recently developed electromagnetic transponders provide real-time three-dimensional (3D) localization without radiation dose, they have much larger physical size than gold markers conventionally used in radiographic tracking and produce severe magnetic resonance imaging artifacts, hindering magnetic resonance–based posttreatment assessment (9). Fluoroscopic imaging with one or two kV sources, on the other hand, poses the problem of accumulating excessive patient imaging dose. Because intrafraction prostate motion is generally unpredictable and patient-specific, model-based approaches are not ideal even with the help of personalized training data acquired right before treatment.

The prostate is mostly stationary and drifts slowly, with abrupt movement occurring only occasionally (4, 10–12). Therefore, in contrast with current motion monitoring techniques that seek to accurately and continuously localize a moving target, in a previous study (13, we attempted for the first step to detect only potential motion beyond a predefined threshold. The method used treatment beam MV imaging available at no cost in tracking dose. In a second step, combined MV-kV imaging was performed by turning on the kV imager to verify the over-threshold event.

Reprint requests: Lei Xing, Ph.D., Radiation Oncology, 875 Blake Wilbur Dr, G233, Stanford, CA 94305-5847. Tel: (650) 498-7896; Fax: (650) 498-4015; E-mail: lei@reyes.stanford.edu

Conflict of interest: None

Supported in part by grants from the DOD PCRP (PC081042) and NCI (CA104205).

Acknowledgment—We thank Drs. P. Kupelian and K. Langen for providing the Calypso data, and Drs. R. Wiersma, W. Mao, S.L. Hancock, C. King, P. Keall, P. Poulsen, and B. Choi for their useful input in this study.

Received July 17, 2009, and in revised form Nov 25, 2009. Accepted for publication Dec 28, 2009.

The second step would also obtain more accurate position information that could be used for interventional motion management by, for example, moving the couch or shifting the MLC. The kV usage was significantly reduced because cine-MV monitoring was sufficient during most of the treatment time. In that work, radiation was delivered in an arc, the ''free'' MV information from different gantry angles was used to stereoscopically estimate 3D prostate/marker coordinates, which in turn were used to detect potential over-threshold displacements. This MV-only 3D localization approach would not appear to apply to real-time displacement estimation during fixed-gantry IMRT, however. Although prostate motion is unpredictable, Calypso (Calypso Medical Technologies Inc, Seattle, WA) real-time monitoring data (3, 4, 10, 11, 14) demonstrated that it is not completely random. The goal of this study is to develop an MV data processing method that is suitable for the ''failure'' detection scheme during IMRT by incorporating simple assumptions based on prior knowledge of prostate motion without introducing complicated statistical models and requiring neither population-based nor pretreatment patient-specific training data.

MATERIALS AND METHODS

Intrafraction prostate motion monitoring strategies for IMRT

One simple way to monitor intrafraction prostate motion without the excessive overhead of continuous kV imaging is to acquire kV with simultaneous MV projections only at the beginning of each IMRT field. Comparison between the results of this approach and those of any proposed method would indicate the motion monitoring efficiency of the method. This approach will be referred to as the ''reference point method'' in the remainder of this article.

The present proposed procedure contains two steps as described previously (13). First, to turn on the kV (for one time or a period of time) only if cine MV-estimation suggest that the marker has moved more than a predefined threshold (3mm) from a previously established checkpoint whose 3D position is known; and then, to update the checkpoint if the MV-kV triangulation confirms that the displacement is more than 2.5 mm. Because of the absence of prior knowledge at the beginning of treatment, the kV imager is turned on one time to acquire the first accurate 3D marker checkpoint position. In this section, we will introduce three different, but related methods for detecting potential over-threshold motion in fixed-gantry IMRT from cine MV. Referring to Fig. 1, let ''L'' be a checkpoint fiducial location, determined by simultaneous MV-kV data. At later times, only cine-MV images are acquired to estimate fiducial displacement from checkpoint L. Let ''P'' be the projected fiducial position on the current MV image. The 3D fiducial position ''M'' to be estimated is along the line joining P and the x-ray source ''F.'' Therefore the fiducial displacement is

$$\overrightarrow{LM} = \overrightarrow{FM} - \overrightarrow{FL} = t \cdot \overrightarrow{FP} - \overrightarrow{FL} \quad (1)$$

where t is a scaling factor to be solved. For the remainder of this article, we assume that the treatment table is parallel to the gantry rotation axis.

Trigger kV imaging using two-dimensional (2D) MV distance. The first method for estimating the fiducial displacement assumes that there is no inline (*i.e.*, perpendicular to imager plane) fiducial

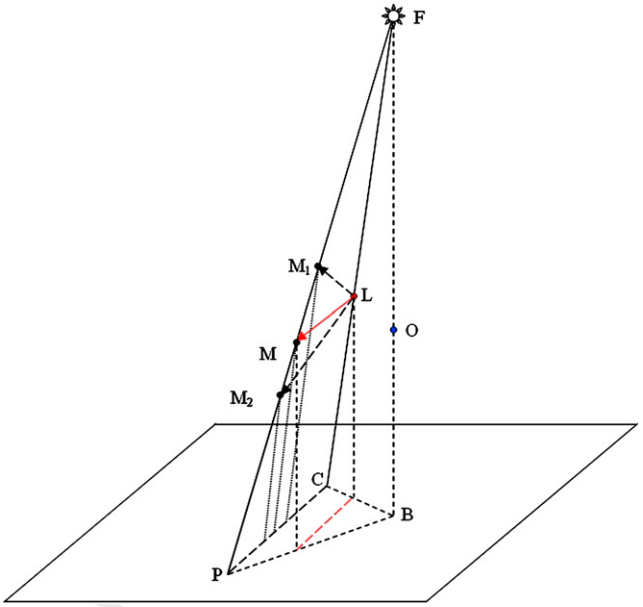

Fig. 1. Projection geometry for estimating fiducial position based on sequential MV images.

motion between the current time and the time when the checkpoint was imaged. It means LM is parallel to the imager, and then motion in the superoinferior (SI) direction may be expressed as

$$\Delta SI \approx \overrightarrow{CP_{SI}} \cdot \frac{|\overrightarrow{FL}|}{|\overrightarrow{FC}|} \quad (2)$$

where $\overrightarrow{CP_{SI}}$ is the $\overrightarrow{CP}$ projected onto the SI direction and C is the projected position of L in the updated MV image. The fiducial position M can be solved using Eq. 1 and 2.

The distance from the fiducial to the isocenter ($\overrightarrow{MO}$) is much smaller than the source-to-axis distance ($\overrightarrow{FO}$). Therefore the estimated 2D motion parallel to the imager ($\overrightarrow{LM}$) is approximately the shortest possible distance from L to the line FP.

Trigger kV imaging using estimated 3D MV distance according to prior knowledge. Knowledge of the characteristics of prostate motion can be readily used to improve 3D motion estimation for over-threshold motion detection. Previous studies show that the lateral motion is significantly smaller than and independent of the vertical and longitudinal motions and the vertical and longitudinal motions are highly correlated, consistent with the pelvis and prostate anatomy (4, 10, 14). Because the SI motion is always perpendicular to the plane of gantry rotation, the SI motion can always be reliably measured from cine MV. Considering all the facts above, we added an estimated inline fiducial motion (*i.e.*, the component of anteroposterior (AP) displacement perpendicular to the imager), as follows:

$$\Delta_{\perp} = \eta \cdot \Delta SI \cdot \cos\alpha \quad (3)$$

where η is an estimated ratio of AP to SI motion ($\Delta AP/\Delta SI$) and α is the gantry angle. The ratio η was updated every time whenever combined data from MV-kV imaging were available. The assumption here is that the ratio does not change significantly during a short period. To avoid the complication of acquiring and being influenced by patient specific training data, no statistical motion model was built. The reason not to do so is that we are only attempting at this stage to detect potential over-threshold motion, not to determine accurate 3D localization. This estimated inline motion was combined

with the calculated in-plane motion as described in the previous section to estimate a 3D fiducial displacement. We did curve fitting and prediction to estimate the possible 3D displacement at the next frame for use in the next step.

The second step of the proposed motion monitoring method was to trigger kV imaging whenever the estimated 3D displacement was greater than a preset threshold. Whether a checkpoint update (repositioning) was performed or not was determined based on the actual fiducial motion measured from the combined MV-kV data. The ratio of AP to SI motion was always updated whenever an MV-kV image pair was taken. Figure 2 is a flowchart of the entire motion monitoring procedure.

Triggering kV imaging using estimated 3D MV distance with information from previous IMRT angle [''3D+ estimation'']. The data from previous treatment angle also provide potential useful information to estimate 3D marker position. In addition to the 3D estimation method, at the beginning of each new gantry angle, we stereoscopically estimated 3D marker position using the current image and last several images from the previous field, assuming no motion between this acquisition and that from the previous gantry angle (13, 15, 16). If the estimated displacement was larger than the preset threshold (invalidating the no-motion hypothesis), then kV imaging would also be triggered. In this way, we give more opportunity for the kV to be turned on when potential large displacement could have happened. The higher probability of large displacement is because the time spent between each beam-on field is relatively long (typically 20–60 s). We anticipate this method would lead to slightly better motion detection performance compared to using only the 3D estimation method (See *Trigger kV imaging using estimated 3D MV distance according to prior knowledge* section). This technique will be hereinafter referred to as the ''3D+ estimation'' method.

Simulation method

To test the current methodology without extensive measurements, a simulation strategy was developed to evaluate the performance of the proposed technique. The simulation geometrically projected a fiducial onto the MV and kV imagers and provided the projected positions as a function of time, which were then used as input for the proposed marker monitoring algorithms to estimate the status of prostate motion. A reliable performance of the imaging system was assumed in the simulation study. In other words, the inaccuracy of the data acquisition system was assumed to be either negligible or correctable through a careful system calibration (17). This assumption had been shown to be reasonable in our previous studies for motion monitoring in arc therapy. A Gaussian detection noise with zero mean and 0.5 pixel standard deviation was added to the projected fiducial positions based on previous phantom measurements of static fiducials (17). In this way, it was found previously (13) that the simulated trajectories were in good agreement with actual experiments.

Case study

The motion monitoring methods were tested with 536 real-time 3D prostate position tracks recorded with implanted electromagnetic transponders (Calypso) from 17 patients (10). We simulated seven-field IMRT (30°, 80°, 130°, 180°, 230°, 280°, 330°) with a 15-s beam-on time during each field and 50 s between beam-on sessions. Therefore, the total track duration was 405 s. The angles and time intervals were chosen based on typical treatments at Stanford Hospital. The original 536 prostate position tracks were used without smoothing in the simulation study.

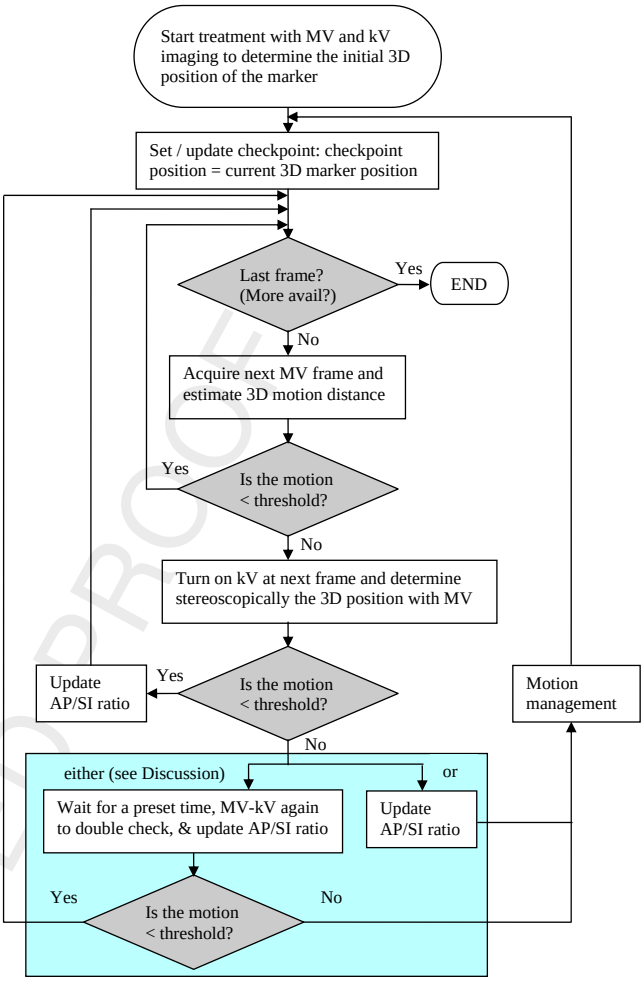

Fig. 2. Flowchart for three-dimensional motion estimation.

RESULTS

Track-specific results

Figure 3 displays a typical example of real-time tracking of a marker obtained using the different approaches discussed in Methods section. During the treatment fraction, the prostate drifted slowly from its original position at the time dose delivery began. Its left-right position did not change noticeably. The trends were similar for SI and AP. Using the ''reference point'' method (Fig. 3b), the kV imager was turned on at the beginning of each field and the over-threshold displacement that occurred during the last delivery field was missed. Because the fiducial position was only measured once using MV-kV triangulation for each field, the estimated displacement appears as horizontal line segments in Fig. 3b. The difference between a red circle and the starting point of the corresponding blue line segment reflects small MV-kV measurement error. With the 2D estimation method, the marker displacement was continuously estimated during dose delivery. MV-estimated displacement was larger than 3 mm at ~403 s; therefore, a kV frame was triggered. Because the simultaneous MV-kV triangulation confirmed that the displacement was larger than the 2.5 mm action threshold, a checkpoint update (repositioning) was performed. Because

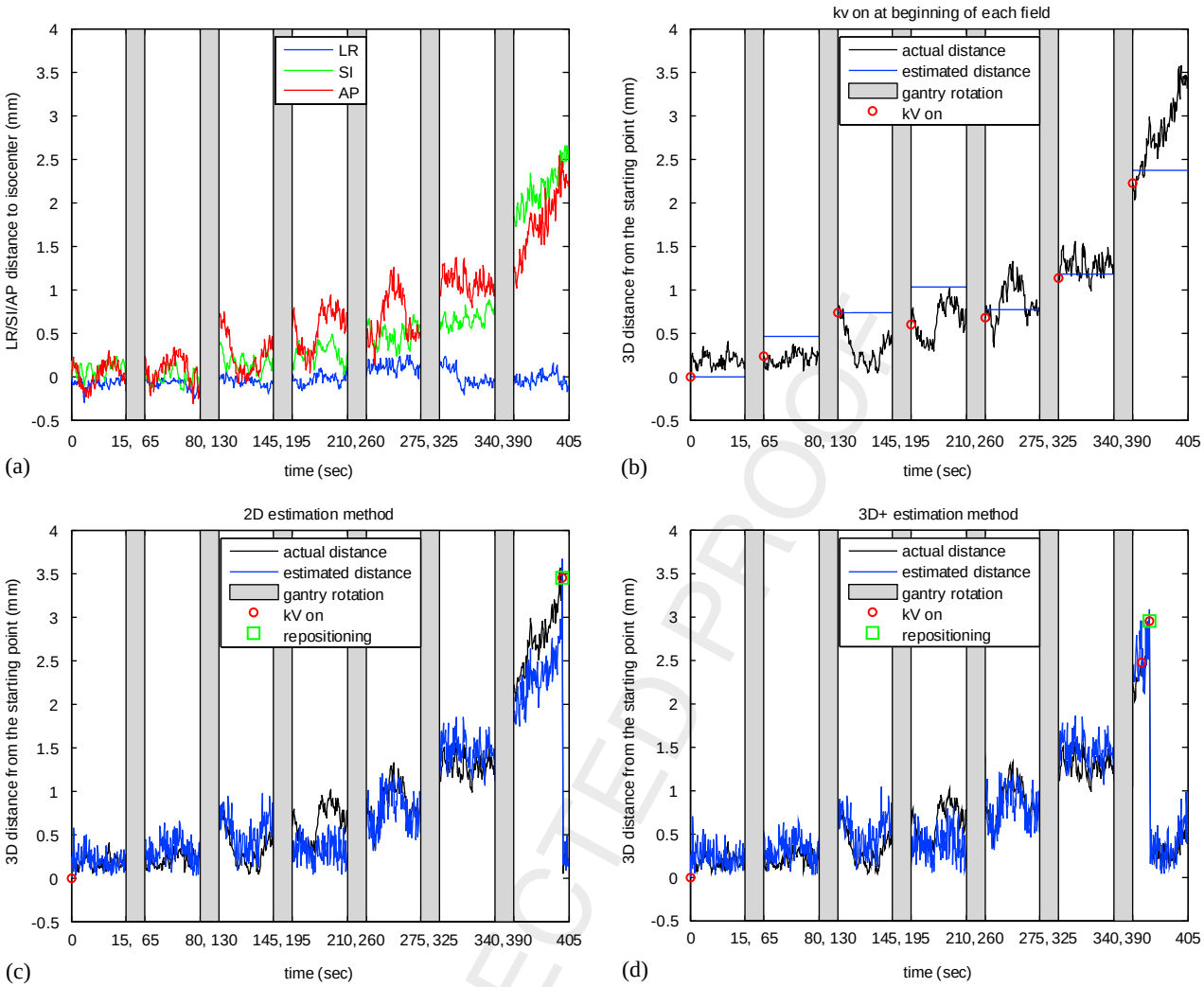

Fig. 3. An example of real-time marker tracking during a seven-field intensity-modulated radiotherapy (IMRT) delivery using different motion monitoring methods. (a) Displays the Calypso-measured patient prostate motion curves in left-right (RL), superoinferior (SI), and anteroposterior (AP) directions. The gray vertical bars represent the times (compressed scale) between IMRT fields when portal imaging was not available. (b–d) The tracking results using the ''reference point,'' ''two-dimensional (2D) estimation,'' and ''three-dimensional (3D)+ estimation'' methods, respectively. (b–d) The black solid traces represent the true vector distance with checkpoint update, the blue solid traces represent the vector distances estimated by the different motion monitoring methods, the red circle symbols show the time at which a kV imaging occurred according to the different estimation algorithms, and the green square symbols denote the checkpoint update events determined from simultaneous MV-kV triangulation. When an update of checkpoint occurs in response to the detected over-threshold marker displacement, it is reflected by a sudden drop of the vector distances.

the 2D estimation assumes no inline motion, it tends to underestimate the displacement, thus the detection of the over-threshold event was delayed. Because the 3D+ estimation method is more extensive than the 2D estimation method, the over-threshold event was immediately detected, and a checkpoint update was done at ~395 s. This example illustrates that the 3D+ estimation method was more accurate than both the 2D estimation and the reference point method in terms of tracking performance. Fewer kV projections were used for the 3D+ estimation method compared to the reference point method.

Although the 3D+ method generally performs better than the other methods, Fig. 4 presents a special case in which both the 2D and 3D+ methods failed to detect an over-threshold displacement, whereas the reference point method detected it successfully. As expected, the 2D method generally underestimated the displacement. The 3D+ method was not helpful in estimating the inline motion because the assumed correlation between AP and SI motions was not present (Fig. 4a). The small SI motion in this case resulted in an underestimate of the AP motion especially when the gantry angle was at ~180° or 360°. The kV imaging was triggered three times at between 261 s and 269 s based on MV estimation. However, none of the over-threshold displacements was confirmed by MV-kV triangulation. The reference point method performed a checkpoint update at 260 s; therefore, the marker was kept in the 3 mm objective of our real-time image guidance during the entire fraction. The reference

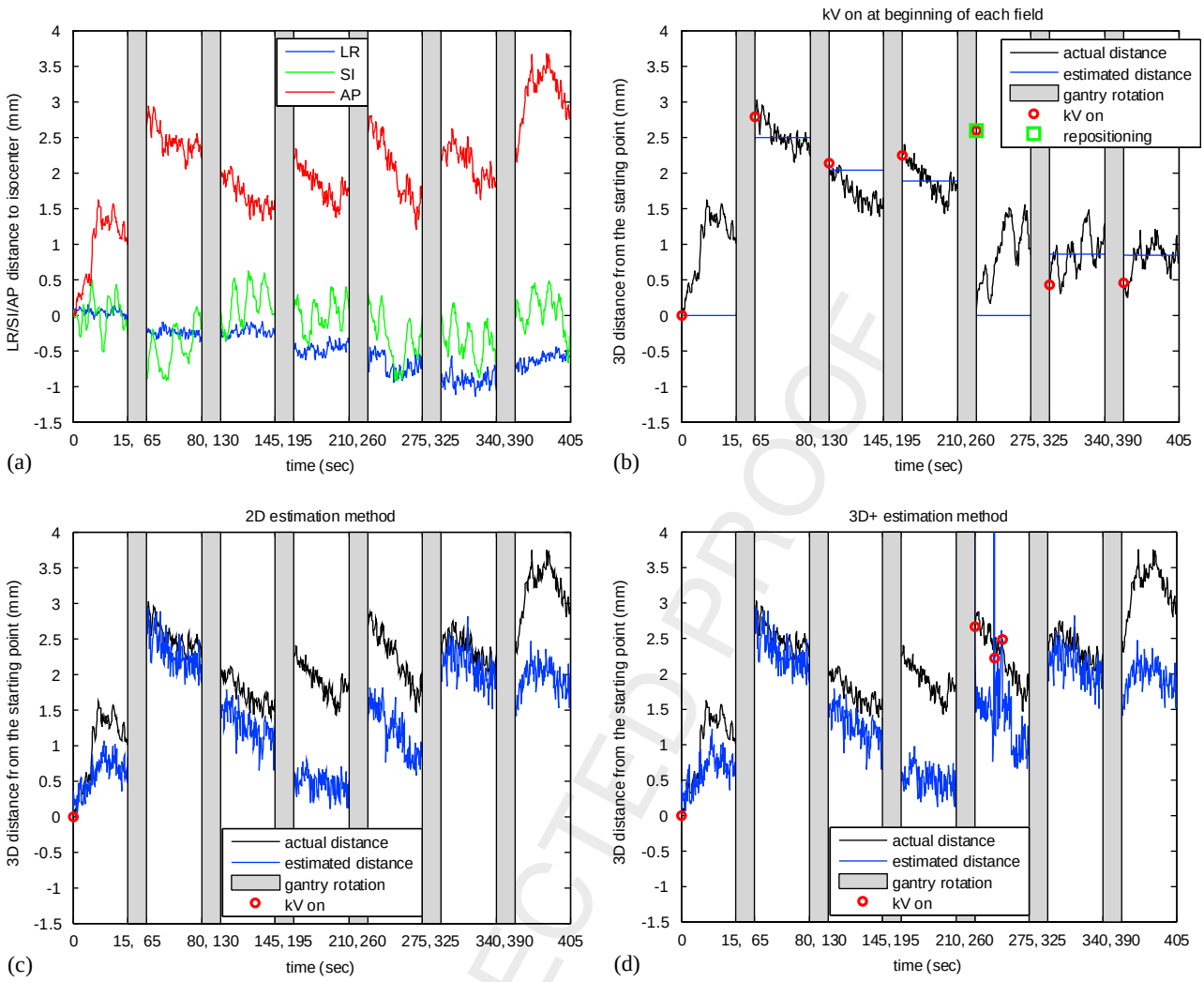

Fig. 4. A special example of real-time marker tracking during a seven-field intensity-modulated radiotherapy delivery using the different motion monitoring methods. Refer to Fig. 3 for captions.

point method did cause more kV images to be taken. An interesting observation for this case is that submillimeter respiration motion was clearly visible in the SI direction.

To evaluate the proposed algorithms, three useful evaluation quantities were studied for the 536 patient tracks as listed in Table 1: the percentage of time that the marker displacement exceeded the preset threshold of 3 mm, which quantified the undetected over-threshold displacement; the number of kV-on events; and the number of checkpoints (or target repositionings) confirmed by simultaneous MV-kV imaging. Of the 536 tracks, 211 (39%) were found to have a displacement greater than 3mm during the ~7 min IMRT treatment fraction. This observation emphasizes the value of the proposed single-imager (MV) estimation technique, because for ~60% of the

Table 1. Track-specific statistical comparison of different motion monitoring strategies comprising all patient data

	Original motion tracks (no intervention)	kV at the beginning of each IMRT field	2D estimation method	3D estimation method	3D+ estimation method
Mean of percentage of over-threshold time*	22.9%	4.9%	3.8%	1.8%	1.5%
Maximum percentage of over-threshold time*	97.2%	38.3%	26.2%	22.9%	14.8%
95th percentile of percentage of over-threshold time*	79.5%	16.2%	14.3%	6.4%	4.3%
Mean number of kV-on per track†	0	7	1.8	2.3	2.5
Mean number of checkpoint update (repositioning) per track†	0	0.49	0.83	1.00	1.02

Abbreviations: 2D = two-dimensional; 3D = three-dimensional; IMRT = intensity-modulated radiotherapy.
* These numbers are obtained based on the 211 3D tracks that contained over-threshold motion.
† These numbers are obtained by averaging over all 536 3D tracks.

fractions, kV imaging is not needed. As shown in Table 1, for the 211 tracks with over-threshold motion, simply taking a simultaneous MV-kV image pair at the beginning of each treatment field reduced the mean percentage of over-threshold time from ~22.9% to ~4.9%. The 2D cine-MV with as-needed kV method used much less kV imaging yet resulted in further (though slight) improvement in target localization efficiency. Based on the prior knowledge that AP and SI prostate motions are correlated, using ''free'' cine-MV information the 3D+ method further reduced the percentage to 1.5% at the cost of a slight increase in kV usage compared with the 2D method. Averaging over all 536 tracks, the proposed 3D+ method kept the fiducial displacement smaller than 3 mm for more than 99.4% of the treatment beam-on time. In the meantime, the average number of kV-on per track was 2.5, which should be considered to be extremely low. The kV usage was only one third of that of the reference point method. The total number of checkpoint update (patient repositioning) events was doubled for the 3D+ approach compared with the reference point method. Together with better timing in checkpoint update, this explains why the percentage of over-threshold time was significantly reduced, even with fewer kV-on times. The non-zero percentage of over-threshold time with the 3D+ estimation method is due to the missed or delayed detection of over-threshold motion for a small number of cases as exemplified in Fig. 4.

Patient-specific results

For each patient, the percentages of time that the marker displacement exceeded the preset 3 mm image guidance objective were averaged over all of that patient's fractions. Figure 5 plots for each patient the averaged percentage of time using the different motion tracking methods. Two patients (number 6 and 15) had very small prostate motion, and for these patients the total over-threshold time was negligible, even without motion tracking. For all the other patients with noticeable amount of over-threshold motion, all motion tracking methods significantly reduced the fractional over-threshold time, with the 3D+ estimation method always being the best. Table 2 lists the mean and maximum percentages over the 17 patients of over-threshold time. It is noteworthy that the maximum patient-specific percentage is only ~1% for the 3D+ estimation method, whereas the corresponding value is as large as ~25% if no motion tracking was performed. Clearly, tracking leads to improvement in dosimetry.

DISCUSSION

Intrafraction organ motion and its management is one of the most important problems to be solved in image guided radiation therapy. Methods to monitor and compensate for intrafraction motion in real time are often resource intensive. Most methods use implanted markers. Current commercially available 3D position monitoring options include stereoscopic x-ray imaging systems (8, 16), which consist of two kV x-ray sources (mounted either on the ceiling or on the gantry) respectively paired with opposed x-ray imagers, and an electromagnetic localization system (Calypso) (3, 4, 10, 11, 14). Usage of the first method has to be weighed against the additional kV imaging dose to which patients are exposed. Severe magnetic resonance imaging artifact from the electromagnetic transponders is a disadvantage of the second approach. More recently, several alternative methods have been reported. For example, Poulsen *et al.* (6) proposed a monoscopic MV imaging technique to monitor prostate motion using a 3D probability density function to resolve the inline motion. Adamson and Wu (5) developed a monoscopic kV imaging approach by registering kV images to template images from CBCT. Combined cine MV and fluoroscopic kV imaging has also been investigated for tracking during IMRT and arc-based therapies (17, 18) with submillimeter tracking accuracy. Q3

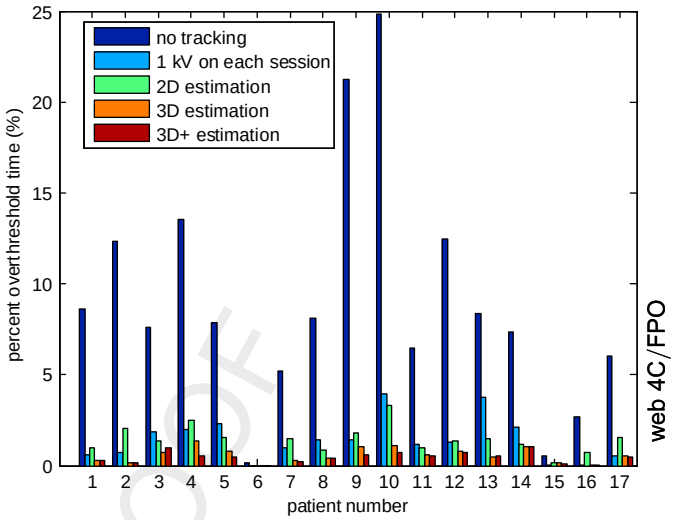

Fig. 5. Total percentage of time that the marker displacement exceeded the preset 3-mm image guidance objective for each patient using the different motion tracking methods.

The characteristics and magnitude of intrafraction motion vary among different organs. Prostate intrafraction motion is notably different from respiratory and cardiac motion. In this study, following the concept of ''failure'' detection as in (13), we proposed a novel fixed-gantry tracking method suitable for the unique features of intrafraction prostate motion. Distinguished from other approaches, this algorithm treats the tracking problem in steps from coarse to fine, because continuously accurate monitoring of the typically slow prostate motion is both costly in dose and unnecessary. The algorithm balances tumor targeting efficiency against unwanted patient dose. According to tracking results for the 3D+ method, allowing prostate displacements greater than 3mm for an average of only ~0.5% of total treatment time corresponds to reducing needed frequency of kV imaging to an average of <3 times per conventional treatment fraction. The 3-mm standard is smaller than margins commonly used in present-day clinics. The undetected over-threshold motions were mainly in the inline direction because the displacements in this direction were estimated whereas those parallel to the MV imager

Table 2. Patient-specific statistical comparison of different motion monitoring strategies

	Original motion tracks (no monitoring)	kV at the beginning of each IMRT field	2D estimation method	3D estimation method	3D+ estimation method
Mean of percentage of over-threshold time	9.03%	1.43%	1.37%	0.57%	0.46%
Maximum percentage of over-threshold time	24.8%	3.96%	3.30%	1.37%	1.04%

Abbreviations: 2D = two-dimensional; 3D = three-dimensional; IMRT = intensity-modulated radiotherapy.

were measured. Dosimetric consequences of uncorrected in-line motions generally are less important than those of over-threshold motions perpendicular to the treatment beam direction.

Upon confirmation of an over-threshold prostate displacement by simultaneous MV-kV data, a number of possible interventional strategies could be implemented to compensate for the motion, including moving the couch or shifting subsequent MLC apertures. The intervention is based on accurate 3D prostate position information which reduces the chance of inappropriate correction as compared to model-based correction (6). Because on average only approximately one intervention per fraction was needed, automatic couch control is well suited for this purpose. The interfacing of current systems with interventional devices is a fit subject for future development.

When multisegmented intensity-modulated MV beams are used for imaging during treatment, a potential difficulty is that the fiducials may be partially or completely blocked by an MLC leaf at certain times. A fiducial blockage avoidance strategy has recently been investigated in the context of a four-dimensional inverse planning study (19). It was shown that it is possible to ensure ''seeing'' at least one of the implanted metallic fiducials in any of the IMRT segments during step-and-shoot dose delivery by adding to the objective function a hard or soft constraint that characterizes the level of preference for the fiducial to be included in the segmented fields. It was found that the final dose distributions of three plans (constraint-free and soft and hard constraints) were very similar, which is understandable because the fiducials are generally placed inside the target volume, or here the prostate. Combined marker and MLC motion with use of multiple markers, leads to possible detection confusion amongst the markers. Efficient use of information from neighboring image frames and application of speed constraints might alleviate the problem.

Short prostate excursion (11) is another concern for the proposed techniques. If a detected over-threshold prostate motion is transient (lasting only a few seconds then moving back), then a repositioning after the detection might be a waste and result in another repositioning seconds later. To avoid this kind of problem, after an over-threshold event is detected, we could wait a certain amount of time, double check whether the excursion is still over the threshold, and reposition if the motion is confirmed again (Fig. 2 flowchart). Additional simulations (not reported in the Results) found negligible performance change by adding a wait time. The number of repositioning events was slightly reduced; however, the percentage of over-threshold time was slightly increased.

Gold marker segmentation can be achieved in real time with relatively high accuracy from simultaneously acquired MV and kV images (20). Based on our experimental results (13), a zero-mean Gaussian fiducial detection noise was added in this study with a standard deviation of 0.5 pixels. Neither geometrical error nor time delay of either imaging or realignment was modeled, however. Although geometrical errors may be minimized by careful system calibration (17), they cannot be completely eliminated. Total time delay may be on the order of 0.5 s (18, 21). Thus the performance in real clinical cases might be slightly degraded. Other the other hand, more sophisticated estimation of fiducial displacement by optimized usage of multiple MV projections at different times and even other prior knowledge from planning CT or CBCT could also be developed. For example, because AP motion is larger than left-right motion, preference of kV imaging may be given at gantry angle $\sim 180^\circ$ and $\sim 360^\circ$. Taking into account all the factors, we do not foresee any major performance degradation in clinical results.

For the proposed 3D+ estimation algorithm, no statistical model is built thus training data are not needed; no complicated optimizations are used, thus real-time decision making is unimpeded. In comparison to other tracking methods, this method has no blockage of the LINAC gantry and in contrast to electromagnetic tracking, the imaging data provide additional anatomical information that might be useful for documentation and retrospective dosimetric evaluation. The methodology and hardware requirements of the present methods are relatively simple, which facilitates their implementation in the clinic. Although some elements are still lacking, this real-time failure detection prostate motion tracking system appears to be feasible. The current simulation study builds a basis for further clinical evaluation.

For patients with implanted fiducials, our department typically uses a $\sim$5 mm clinical target volume to planning target volume margin with reduction to $\sim$3 mm posteriorly to avoid the rectum based on individual anatomy. This margin gives sufficient tumor targeting accuracy (14). Our proposed method is towards margin reduction to reduce the dose to organs at risk to enable benefits from dose escalation.

In summary, we have demonstrated that efficient real-time intrafraction prostate motion tracking with reasonable tumor targeting accuracy is achievable using cine MV with minimal as-needed kV imaging. We anticipate that the proposed technique will be clinically practical and would be beneficial for IMRT prostate cancer treatment.

REFERENCES

1. Soete G, De Cock M, Verellen D, *et al*. X-ray-assisted positioning of patients treated by conformal arc radiotherapy for prostate cancer: Comparison of setup accuracy using implanted markers versus bony structures. *Int J Radiat Oncol Biol Phys* 2007;67:823–827.
2. Kotte ANTJ, Hofman P, Lagendijk JJW, *et al*. Intrafraction motion of the prostate during external-beam radiation therapy: Analysis of 427 patients with implanted fiducial markers. *Int J Radiat Oncol Biol Phys* 2007;69:419–425.
3. Noel C, Parikh PJ, Roy M, *et al*. Prediction of intrafraction prostate motion: Accuracy of pre- and post-treatment imaging and intermittent imaging. *Int J Radiat Oncol Biol Phys* 2008. Q4
4. Kupelian P, Willoughby T, Mahadevan A, *et al*. Multi-institutional clinical experience with the Calypso System in localization and continuous, real-time monitoring of the prostate gland during external radiotherapy. *Int J Radiat Oncol Biol Phys* 2007;67:1088–1098.
5. Adamson J, Wu Q. Optimizing monoscopic kV fluoro acquisition for prostate intrafraction motion evaluation. *Phys Med Biol* 2009;54:117–133.
6. Poulsen PR, Cho B, Langen K, *et al*. Three-dimensional prostate position estimation with a single x-ray imager utilizing the spatial probability density. *Phys Med Biol* 2008;53:4331–4353.
7. Balter JM, Wright JN, Newell LJ, *et al*. Accuracy of a wireless localization system for radiotherapy. *Int J Radiat Oncol Biol Phys* 2005;61:933–937.
8. Britton KR, Takai Y, Mitsuya M, *et al*. Evaluation of inter- and intrafraction organ motion during intensity modulated radiation therapy (IMRT) for localized prostate cancer measured by a newly developed on-board image-guided system. *Radiat Med* 2005;23:14–24.
9. Xing L, Lee L, Timmerman R. Image guided adaptive radiation therapy and practical perspectives. In: Timmerman R, Xing L, editors. Image guided and adaptive radiation therapy. Philadelphia: Lippincott Williams & Wilkins; 2009.
10. Langen KM, Willoughby TR, Meeks SL, *et al*. Observations on real-time prostate gland motion using electromagnetic tracking. *Int J Radiat Oncol Biol Phys* 2008;71:1084–1090.
11. Malinowski KT, Noel C, Roy M, *et al*. Efficient use of continuous, real-time prostate localization. *Phys Med Biol* 2008;53:4959–4970.
12. Xie Y, Djajaputra D, King CR, *et al*. Intrafractional motion of the prostate during hypofractionated radiotherapy. *Int J Radiat Oncol Biol Phys* 2008;72:236–246.
13. Liu W, Wiersma R, Xing L. Optimized hybrid MV-kV imaging protocol for volumetric prostate arc therapy. *Int J Radiat Oncol Biol Phys* 2009;revised. Q5
14. Li HS, Chetty IJ, Enke CA, *et al*. Dosimetric consequences of intrafraction prostate motion. *Int J Radiat Oncol Biol Phys* 2008;71:801–812.
15. Aubry JF, Beaulieu L, Girouard LM, *et al*. Measurements of intrafraction motion and interfraction and intrafraction rotation of prostate by three-dimensional analysis of daily portal imaging with radiopaque markers. *Int J Radiat Oncol Biol Phys* 2004;60:30–39.
16. Berbeco RI, Jiang SB, Sharp GC, *et al*. Integrated radiotherapy imaging system (IRIS): Design considerations of tumour tracking with linac gantry-mounted diagnostic x-ray systems with flat-panel detectors. *Phys Med Biol* 2004;49:243–255.
17. Liu W, Wiersma RD, Mao W, *et al*. Real-time 3D internal marker tracking during arc radiotherapy by the use of combined MV-kV imaging. *Phys Med Biol* 2008;53:7197–7213.
18. Wiersma RD, Mao WH, Xing L. Combined kV and MV imaging for real-time tracking of implanted fiducial markers. *Med Phys* 2008;35:1191–1198.
19. Ma Y, Lee L, Keshet O, *et al*. Four-dimensional inverse treatment planning with inclusion of implanted fiducials in IMRT segmented fields. *Med Phys* 2009;36:2215–2221.
20. Mao W, Riaz N, Lee L, *et al*. A fiducial detection algorithm for real-time image guided IMRT based on simultaneous MV and kV imaging. *Med Phys* 2008;35:3554–3564.
21. Sweeney RA, Arnold W, Steixner E, *et al*. Compensating for tumor motion by a 6-degree-of-freedom treatment couch: is patient tolerance an issue? *Int J Radiat Oncol Biol Phys* 2009;74:168–171.

Int. J. Radiation Oncology Biol. Phys., Vol. ■, No. ■, pp. 1–10, 2010

0360-3016/$–see front matter

ELSEVIER

doi:10.1016/j.ijrobp.2009.11.056

CLINICAL INVESTIGATION

OPTIMIZED HYBRID MEGAVOLTAGE-KILOVOLTAGE IMAGING PROTOCOL FOR VOLUMETRIC PROSTATE ARC THERAPY

WU LIU, PH.D.,* RODNEY D. WIERSMA, PH.D.,* AND LEI XING, PH.D.*

*Department of Radiation Oncology, Stanford University School of Medicine, Stanford, California

Purpose: To develop a real-time prostate position monitoring technique for modern arc radiotherapy through novel use of cine-megavoltage (MV) imaging, together with as-needed kilovoltage (kV) imaging.
Methods and Materials: We divided the task of monitoring the intrafraction prostate motion into two steps for rotational deliveries: to detect potential target motion beyond a predefined threshold using MV images from different viewing angles by taking advantage of gantry rotation during arc therapy and to verify the displacement and determine whether intervention is needed using fiducial/tumor position information acquired from combined MV-kV imaging (by turning on the kV imager). A Varian Trilogy linear accelerator with an onboard kV imager was used to examine selected typical trajectories using a four-dimensional motion phantom. The performance of the algorithm was evaluated using phantom measurements and computer simulation for 536 Calypso-measured tracks from 17 patients.
Results: Fiducial displacement relative to the MV beam was limited to within a range of 3 mm 99.9% of the time with <1 mm accuracy. On average, only ~0.5 intervention per arc delivery was needed to achieve this level of accuracy. Compared with other fluoroscopy-based tracking techniques, kV use was significantly reduced to an average of <15 times per arc delivery.
Conclusion: By focusing the attention on detecting predefined abnormal motion (*i.e.*, "failure" detection) and using the inherent mechanism of gantry rotation during arc radiotherapy, the current approach provides high confidence regarding the prostate position in real time without the unwanted overhead of continuous or periodic kV imaging. © 2010 Elsevier Inc.

Intrafraction prostate motion, onboard imaging, volumetric arc therapy.

INTRODUCTION

Numerous studies (1–6) have shown that the prostate target moves during the radiotherapy dose delivery process and that the motion is generally unpredictable and can be >1 cm in some cases. Real-time monitoring of implanted fiducial markers using cine-megavoltage (MV) and onboard kilovoltage (kV) beams has been proposed for real-time monitoring of tumor target motion (7, 8). Although continuous fluoroscopic kV and cine-MV imaging is capable of providing real-time information of the prostate position, with spatial accuracy <1 mm, a practical issue has been whether it is necessary to keep kV imaging on continuously to monitor the prostate motion, which only occurs sporadically. A reliable reduction of kV beam use would be highly desirable to reduce the patient imaging dose (9).

If the therapeutic dose is delivered in an arc, the fiducial marker/tumor positions can be stereoscopically estimated by taking advantage of the inherent mechanism of continuous gantry rotation. This is done with the analysis of the ''free'' MV images acquired from different angles and forms a rational basis to minimize kV use. During arc therapy, the MV projections corresponding to different points in time (gantry angles) do not provide the full three-dimensional (3D) coordinates of the fiducial markers. However, with an adequately established baseline position of the prostate at the beginning of treatment, they can potentially determine whether the

Reprint requests to: Lei Xing, Ph.D., Department of Radiation Oncology, Stanford University School of Medicine, 875 Blake Wilbur Dr., Stanford, CA 94305-5847. Tel: (650) 498-7896; Fax: (650) 498-4015; E-mail: lei@stanford.edu

Presented at the 51st Annual Meeting of the American Association of Physicists in Medicine (AAPM), July 26-30, 2009, Anaheim, CA.

Supported in part by the Department of Defense Prostate Cancer Research Program (Grants PC081042 and PC073690) and National Cancer Institute (Grant CA104205).

Conflict of interest: none.

R. D. Wiersma is currently at the Department of Radiation and Cellular Oncology, University of Chicago Medical Center, Chicago, IL.

Conflict of interest: none.

Acknowledgments—We thank Drs. P. Kupelian and K. Langen for providing the Calypso data, and Drs. G. Luxton, P. Keall, P. Poulsen, B. Choi, C. King, S. L. Hancock, and W. Mao for their help with the experiments.

Received Sept 18, 2009, and in revised form Nov 11, 2009. Accepted for publication Nov 12, 2009.

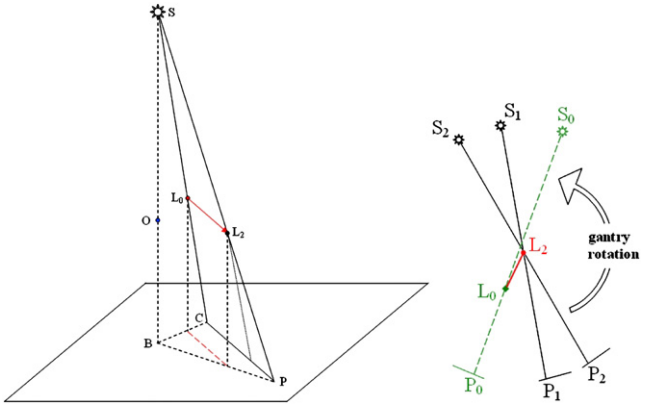

Fig. 1. Projection geometry (Left) and estimation of fiducial position using sequential megavoltage projections (Right).

prostate has moved from the baseline position and whether the displacement is greater than a preset threshold (*e.g.*, ~3 mm). The estimated displacement of the prostate target using the MV projections at different points can be used to direct the use of orthogonal kV imaging. If a potential overthreshold motion is detected by MV imaging, kV imaging can be used (for a single shot or a certain period) to accurately locate the 3D prostate position using simultaneous MV-kV imaging for possible intervention. The goal of the present study was to develop such an MV data processing method and optimal kV imaging protocol for arc therapy. The scheme of using the kV imager on an ''as needed'' basis has the potential to significantly improve the current ''one-protocol-for-all-treatment'' approach of prostate image-guided radiotherapy.

METHODS AND MATERIALS

MV-kV imaging

Three methods can be used to combine kV imaging with cine-MV imaging to monitor implanted gold seeds during prostate image-guided radiotherapy. These include continuous kV imaging (7); periodic kV according to previously established prostate motion statistics; and using kV imaging only if the estimated prostate displacement or speed from the up-to-date MV projections has exceeded a threshold. The first two methods are in the category of ''one-protocol-for-all-treatment.'' The present study focused on the development of the third approach. Because of the random and relatively infrequent nature of prostate motion, as will be seen in the following sections, the third approach can outperform the first two by reducing kV use while maintaining a high level of marker tracking accuracy compared with continuous kV imaging.

Prostate motion detection using cine-MV and as-needed kV projections

The central idea of the proposed strategy is to estimate the fiducial displacement using MV-only data by taking advantage of the continuous gantry rotation during arc therapy, using the kV imager only with the detection of possible abnormal motion. Therefore, we divided the task of monitoring intrafraction prostate motion into two separate, but related, steps: first, to detect any abnormal target motion through continuously updated MV images; and, second, to confirm and accurately locate the fiducial markers using the kV imager

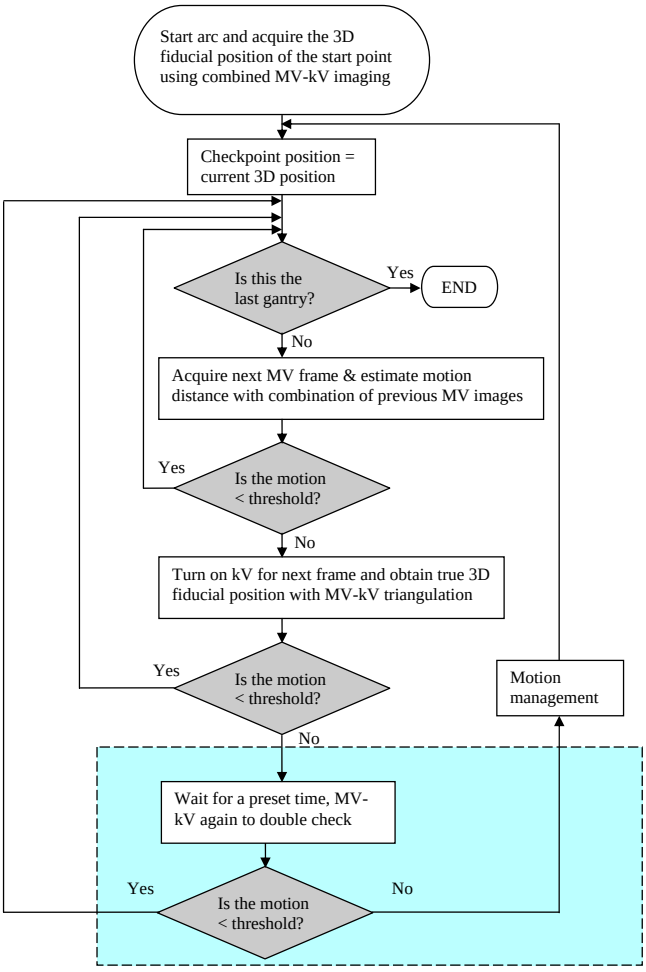

Fig. 2. Flowchart of prostate motion monitoring and intervention using cine-megavoltage and as-needed kilovoltage imaging.

only if a potential abnormal motion were detected. The accurate position information would then be used to guide additional intervention. The MV imaging geometry is sketched in Fig. 1. At a gantry angle, the projection point of the marker on the MV electronic portal imaging device plane (Point P) is along the ray joining the X-ray source (S) and the marker (L_2). To determine or estimate the 3D marker position, (x, y, z), a triangulation of two projections is required. One MV image provides two known parameters; therefore, at least one more constraint is needed to solve for the three unknown coordinates. This additional constraint can come from either a kV image or another MV image acquired at a different gantry angle.

Figure 2 shows a flowchart of the proposed motion management procedure. Because of the absence of previous knowledge at the beginning of treatment, the kV imager should be turned on once to acquire the first accurate 3D marker position. These data can also come from the patient setup images, provided the elapsed time between the setup and treatment has been sufficiently short.

Displacement estimation using MV projections at different times. Referring to Fig. 1, let the fiducial position be L_0, determined by simultaneous MV-kV imaging at time t_0. At later times, only cine-MV images will be acquired to estimate the fiducial displacement from checkpoint L_0. Let S_0, S_1, and S_2 represent the X-ray source positions at t_0, t_1, and t_2, and their projections of the fiducial on the imager at P_0, P_1, and P_2, respectively. The task is to estimate whether the fiducial marker has moved from L_0 more than the predefined threshold at t_2 as determined from its projection position P_2 and

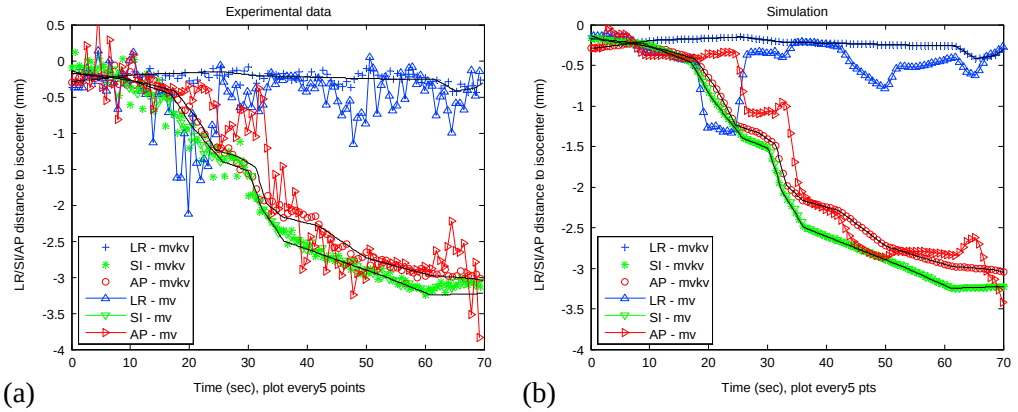

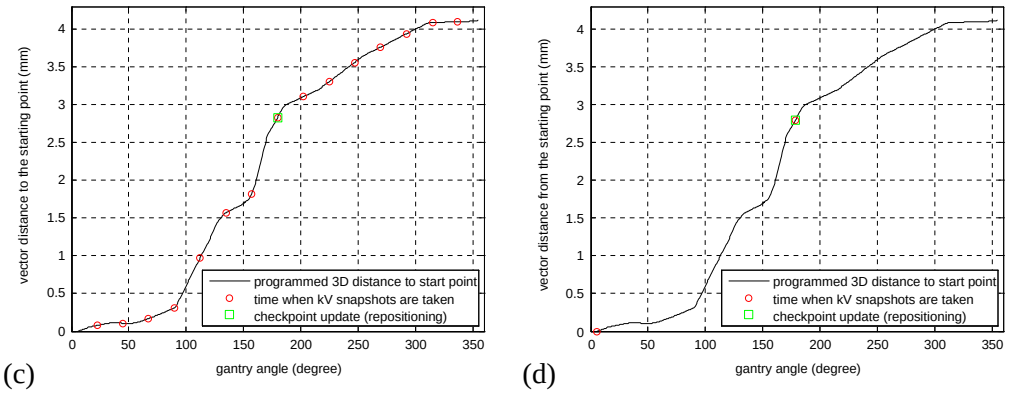

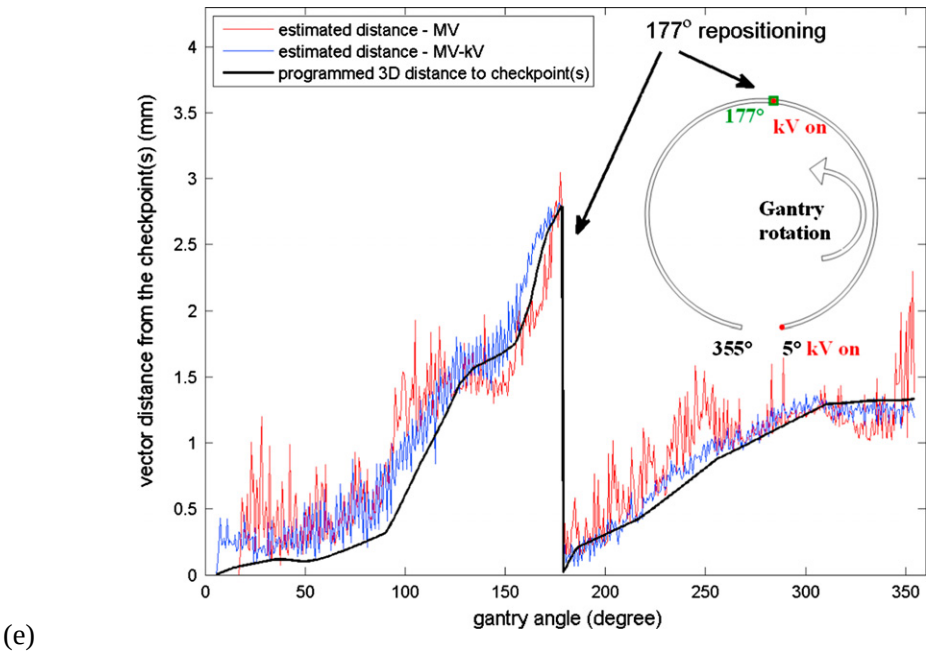

Fig. 3. Real-time marker tracking using different methods for motion type ‘‘continuous target drift.’’ (a) Experimental and (b) simulation results. Solid black curves represent Calypso-measured tracks. Cross, star, and circle indicate results in left–right (LR), superoinferior (SI), and anteroposterior (AP) directions obtained using previously established method of continuous (7.5-Hz) simultaneous megavoltage (MV)-kilovoltage (kV) imaging (7). Triangles indicate marker positions estimated using cine-MV method. (c) Periodic MV-kV triangulation (every 22.5°) and (d) proposed technique. Red circles indicate gantry angle/time when kV imaging was switched on; green squares denote checkpoint update (repositioning) event determined by MV-kV data. (e) Black solid curve shows ground truth vector distance with checkpoint update in proposed method. Red and blue curves indicate tracks derived from proposed method and continuous MV-kV method, respectively. Update of checkpoint occurred at ∼177° in response to detected overthreshold marker displacement, reflected by sudden decrease in vector distance curves.

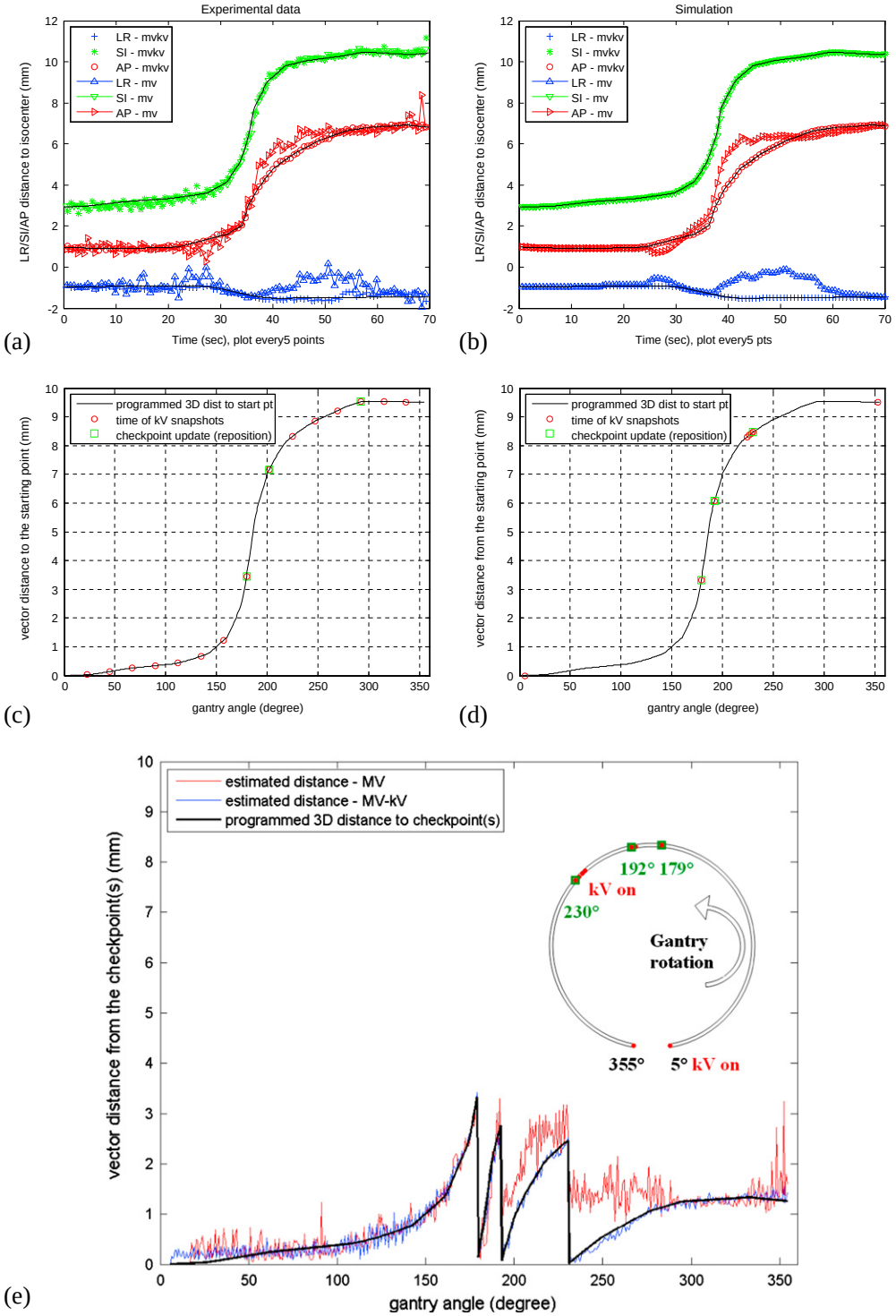

Fig. 4. Real-time marker tracking using different methods for motion type ''persistent excursion.'' (a) Experimental and (b) simulation results. Solid black curves represent Calypso-measured tracks. Cross, star, and circle indicate results in left–right (LR), superoinferior (SI), and anteroposterior (AP) directions obtained using previously established method of continuous (7.5-Hz) simultaneous megavoltage (MV)-kilovoltage (kV) imaging (7). Triangles indicate marker positions estimated using cine-MV method. (c) Periodic MV-kV triangulation (every 22.5°) and (d) proposed technique. Red circles indicate gantry angle/time when kV imaging was switched on; green squares denote checkpoint update (repositioning) event determined by MV-kV data. (e) Black solid curve shows ground truth vector distance with checkpoint update in proposed method. Red and blue curves indicate tracks derived from proposed method and continuous MV-kV method, respectively.

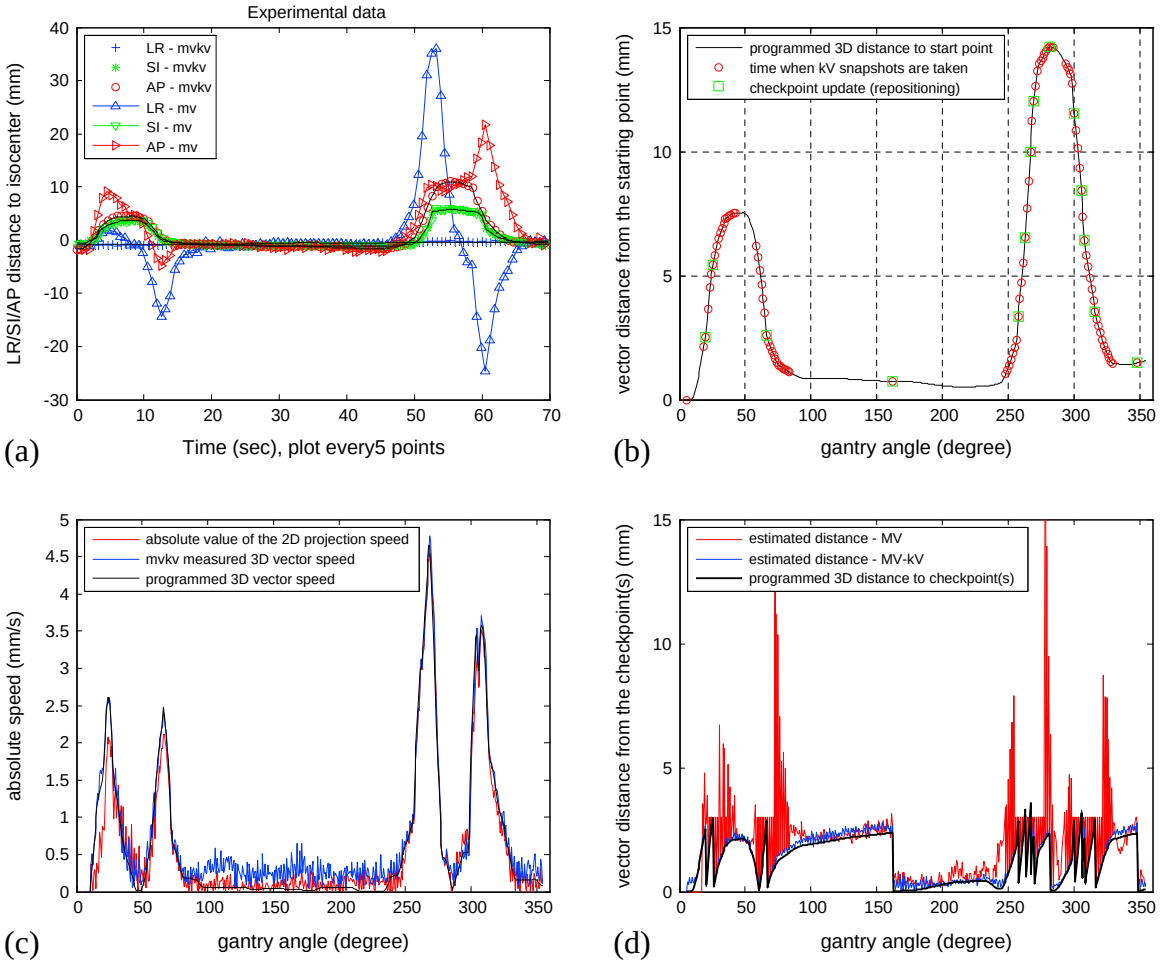

Fig. 5. Real-time marker tracking using different methods for motion type ''high-frequency excursion.'' (a) Experimental results. Solid black curves represent Calypso-measured tracks. Cross, star, and circle indicate results in left–right, superoinferior, and anteroposterior directions obtained using previously established method of continuous (7.5-Hz) simultaneous megavoltage (MV)-kilovoltage (kV) imaging (7). Triangles indicate marker positions estimated using cine-MV method. (b) Motion monitoring strategy using proposed method. Red circles indicate gantry angle/time when kV imaging was switched on; green squares denote checkpoint update (repositioning) event determined by MV-kV data. (c) Red curve shows absolute value of two-dimensional projection motion speed of marker (see Appendix 4). For comparison, programmed and continuous MV-kV–measured three-dimensional speed also displayed as black and blue curves, respectively. (d) Three-dimensional vector distances to checkpoints. Black solid curve shows ground truth vector distance with checkpoint update in proposed method. Red and blue curves indicate tracks derived from proposed method and continuous MV-kV method, respectively.

other system information. To locate the position of the marker at t_2, a projection different from S_2P_2 is necessary. During gantry rotation, cine-MV images are acquired from a wide variety of angular views. Thus, the projection acquired at an earlier time (t_1) is used as the second projection for estimation of the extent of prostate motion. Because t_1 and t_2 correspond to two different points, the triangulation of S_1P_1 and S_2P_2 will not be meaningful unless the marker motion is insignificant during the sampling interval between t_1 and t_2. As long as this interval is sufficiently small (*i.e.,* less than the average time for the prostate to move significantly, 2 mm), the triangulation should provide a reasonable estimate of the marker position. However, the angular separation between two MV images should not be too small. Otherwise, the reconstruction would be too susceptible to image noise and other small errors in the projection data. Theoretical and experimental studies (Appendices 1–3) have shown that an $\sim 10^\circ$ separation is a balanced choice for prostate motion monitoring. It usually takes 2–3 s for the gantry to rotate 10° during arc delivery. The distance L_0L_2 obtained using S_1P_1 and S_2P_2 with 10° separation provides a reasonable estimate of the marker displacement with respect to the checkpoint L_0. If L_0L_2 is >3 mm, kV imaging is triggered to more accurately locate the fiducial marker. The checkpoint is updated (*e.g.,* the target is repositioned or the multileaf collimator [MLC] is shifted) if the MV-kV image confirms the overthreshold movement. With an objective accuracy of image guidance <3 mm, we set the MV-kV action level for checkpoint update at 2.5 mm to count for various uncertainties. Using an action level of <3 mm enhanced our confidence level in catching overthreshold motion, although at the cost of a slightly increased number of checkpoint repositioning events.

High-speed motion. This estimation method is well suited for slow prostate motion in which the displacement corresponding to the two projections is less than $\sim$2 mm within any $\sim$2-second duration, representing most of the clinical situations (as presented in the ''Results'' section, this is true 99.5% of the time). In some rare, but possible situations, the prostate might move more than a few millimeters each second (*e.g.,* because of passing gas in the rectum).

Although this estimation does not yield accurate results because the marker positions are dramatically different at the two points at which the projections were taken, it can be used to reliably detect potential large displacements most of the time. kV imaging was also triggered when the projected fiducial motion speed on the MV imager was large because this indicates that the MV-only localization is not accurate. In the proposed method, the kV-on action was prompted if the MV pair-derived displacement was >3 mm (regardless of the speed value) or if the MV-estimated displacement was >2 mm and the MV-estimated fiducial two-dimensional projection speed was >1 mm/s. Appendix 4 presents more detailed descriptions on managing high-speed motion.

Experimental and simulation studies

The performance of the prostate motion detection technique was evaluated experimentally using an 8-cm cubic plastic phantom placed on a motion platform (Washington University, St. Louis, MO). An arc plan (5–355°) was delivered to the phantom with an embedded ball bearing 3 mm in diameter. The source-to-imager distance for both MV and kV was 150 cm. The MV and kV experimental setup have been previously described in detail (7). Three typical tracks (i.e., continuous target drift, persistent excursion, and high-frequency excursion) (3) were used to program the motion trajectories of the test phantom. They were selected from 536 prostate motion tracks recorded with implanted electromagnetic transponders (Calypso Medical Technologies, Seattle, WA) from 17 patients (5). The experiments were repeated twice for each track to confirm reproducibility. The estimated positions using the proposed method were compared with the known trajectories.

To validate the current method without extensive measurements, a simulation strategy was developed to further evaluate the performance of the proposed technique. The simulation geometrically projected a fiducial marker onto the MV and kV imagers and provided the projected positions as a function of time. The projected positions were then used as input for the proposed marker monitoring algorithms to estimate the prostate motion status. The inaccuracy of the data acquisition system was assumed to be either negligible or correctable through careful system calibration (7). A gaussian detection noise with a mean of 0 pixels and standard deviation of 0.5 pixel was, however, added to the projected fiducial positions, which was reasonable according to previous phantom measurements of static fiducial markers (7).

Computer simulations were performed for all the 536 continuous Calypso-measured prostate position tracks. We assumed a 5°/s gantry rotation speed in our simulation studies. As shown in the ''Results'' section, the simulation strategy was found to be valid because the phantom measurements were very similar to those from the simulations.

RESULTS

The data of real-time tracking of a marker obtained using different approaches for a motion type of ''continuous target drift'' are summarized in Fig. 3 (3). The experimental and simulation results are displayed. The measured data using the MV-pair method showed a high-frequency fluctuation of 0.5–1 mm in amplitude, which was attributed to the position reconstruction noise and other uncertainties in fiducial detection. Such fluctuation was not seen in the simulation study (Fig. 3b), because the random detection noise was not added to show the small difference between an ideal simulation and the real measurements. The simulated and measured positions had similar behavior, and both tracks were very close to the reference input motion. Because our goal of prostate motion monitoring was to keep the marker position within 3 mm of a previously determined checkpoint, 3D displacement of the fiducial markers (with respect to the fiducial's initial position) was more relevant (Fig. 3c–e). The proposed method caught the overthreshold displacement immediately and prompted the kV-on signal thereafter (Fig. 3d).

In contrast, when the periodic (22.5° interval) MV-kV method was used for motion monitoring, this large displacement was not detected until the gantry had rotated to 180° (Fig. 3c). It was a coincidence that the periodic MV-kV method detected the large displacement at a gantry angle of 180°, not too far from 177°. The situation might have been worse if the large motion had occurred, for instance, right after 180° because the displacement would not have been detected until the gantry had rotated to 202.5°) or if the kV imaging was on less frequently.

In this example case, the threshold was reached only once during the whole delivery process. Owing to the lack of guidance in the periodic kV-on method, the kV imager was switched on 15 times during arc delivery. Because of the more intelligent use of the kV system, the proposed approach significantly reduced the use of the kV beam compared with a continuous (7) or periodic kV-on scheme.

An analysis of the 536 Calypso tracks indicated that 98.5% of the time, the prostate did not move >1 mm (99.5% of the time, it did not move >2 mm) in any 2-second duration. This suggests that most prostate patient motions are slow and can be efficiently monitored using the cine-MV method (Fig. 3). A ''persistent excursion'' case is presented in Fig. 4. In that case, the displacement was rather large (~9 mm), occurring between gantry angles 150° and 250° (~20 s). Once again, the experimental and simulation results closely reproduced the Calypso track. The periodic kV-on of every 22.5° was not sufficient to detect all the overthreshold displacements in time, although the proposed method caught all three overthreshold displacements reliably without delay. Three unnecessary kV-on alerts occurred at angles between 225° and 230° that were caused by the fluctuation in the cine-MV displacement estimation. As shown in Fig. 4e, the MV-pair estimated displacement reached 3 mm three times (red curve) before the MV-kV measurement confirmed the displacement (blue curve) had reached the 2.5-mm action level and triggered a checkpoint update (repositioning). The total number of kV snapshot requests triggered by cine-MV estimation was eight for this case, one-half the number used in the periodic (every 22.5°) kV-on scheme. Not only was the kV use reduced, but also the tumor targeting performance was improved.

The prostate motions we have presented were slow and the speed criterion described in section ''High-speed motion'' was not triggered. The experimental results for a motion type of high-frequency excursion are shown in Fig. 5. The simulation study yielded similar results (data not shown). The marker speed parallel to the MV imaging plane (two-dimensional projection speed) is plotted in Fig. 5c, along with

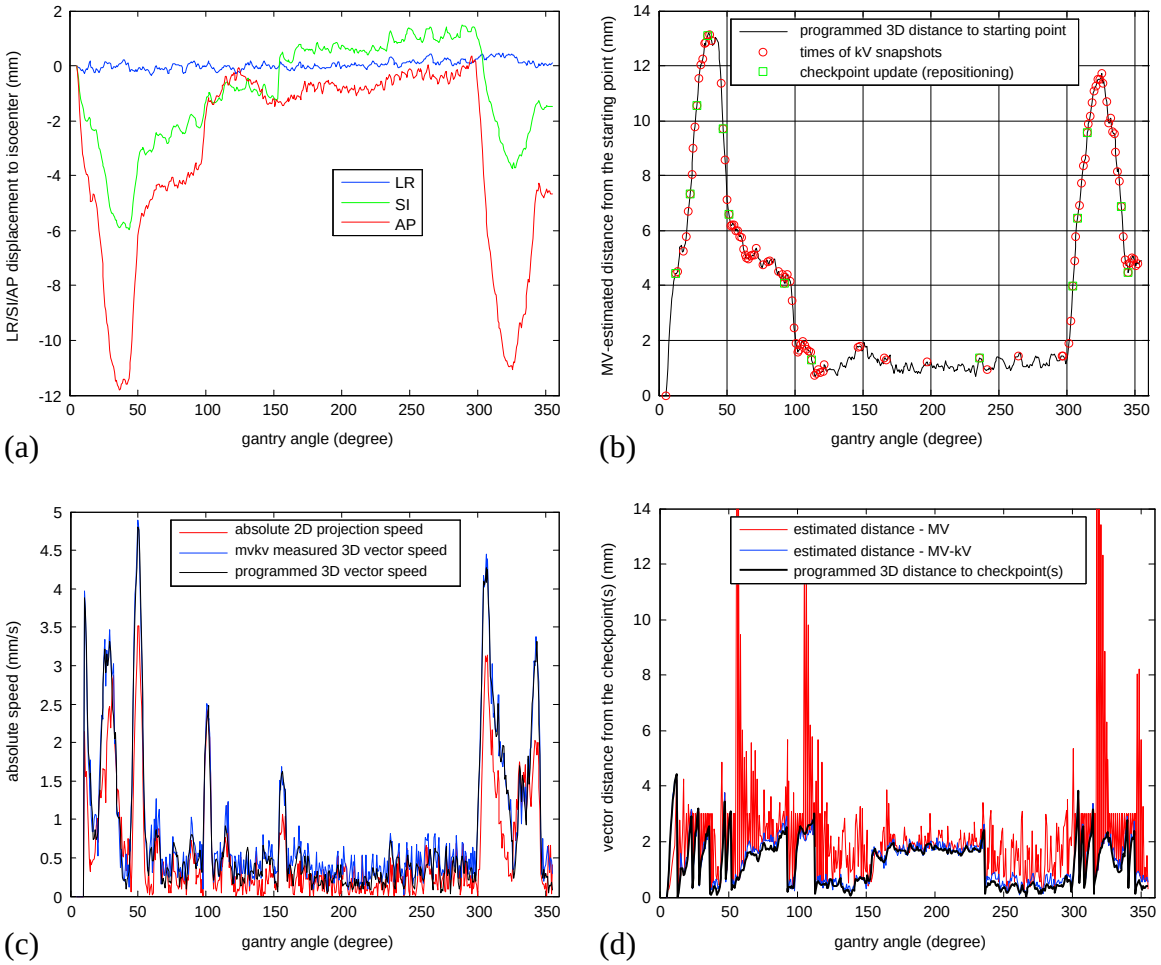

Fig. 6. (a) Calypso-measured prostate coordinates in left–right (LR), superoinferior (SI), and anteroposterior (AP) directions. (b) Motion monitoring strategy using proposed method. Red circles indicate gantry angle/time when kilovoltage (kV) imaging was switched on; green squares denote checkpoint update (repositioning) event determined by megavoltage (MV)-kV data. (c) Motion speed estimations. Red curve shows absolute value of two-dimensional projection motion speed of marker (see Appendix 4). For comparison, programmed and continuous MV-kV–measured three-dimensional speed also displayed as black and blue curves, respectively. (d) Three-dimensional vector distances. Black solid curve shows ground truth vector distance with checkpoint update in proposed method. Red and blue curves indicate tracks derived from proposed method and continuous MV-kV method, respectively.

the 3D vector speed derived from the programmed motion and continuous MV-kV measurements. In general, the two-dimensional projection speed reasonably reflected the motion behavior of the marker. In this case, the fiducial moved rapidly once in a while, leading to large MV-estimation errors (track reconstruction artifacts). With the use of a speed criterion (*i.e.,* requesting the kV-on when the projection speed was >1 mm/s), the cine-MV method rapidly detected fast and large motions happening at ∼5 s (∼30°) and ∼50 s (∼250°).

Figure 6 shows the simulation study of an extreme track in which the 3-mm threshold was exceeded 25.9% of the time when the periodic (22.5° interval) MV-kV method was used. This was reduced to 1.7% using the current approach, resulting in significantly better beam targeting. Thus, sudden large displacements can be detected more effectively using the proposed approach than using the periodic MV-kV imaging (22.5° interval) method. This is understandable because the cine-MV imaging continuously estimates the marker displacement and triggers kV imaging as needed. In contrast, the periodic MV-kV method acquires marker position information only at fixed points.

Finally, the simulation results using all 536 Calypso-measured tracks are summarized in Table 1. Again, the simulation strategy was verified by the experimental results; thus, the simulation was valid for evaluating the proposed method. Three useful evaluation quantities listed in Table 1 the percentage of time that the marker displacement exceeded the preset threshold of 3 mm, which quantified the undetected/uncorrected overthreshold displacement; the number of kV-on events; and the number of checkpoints (repositionings) confirmed by simultaneous MV-kV imaging. Of the 536 tracks, only 74 had a displacement of >3 mm, partly because only the first 70 s of ∼10 min of the tracks in the original studies (4, 5) were used. This observation highlights the importance of the proposed cine-MV approach. The results imply that continuously or periodically switching the kV system on has been overused for most treatment fractions in prostate

Table 1. Comparison of different motion monitoring strategies

Variable	Original motion tracks (no monitoring)	kV on at 5°, 45°, 90°, 135°, …, 315°	kV on at 5°, 22.5°, 45°, 67.5°, …, 337.5°	Proposed method
Mean percentage of overthreshold time* (%)	21.4	6.0	4.0	0.4
Maximum (95th percentile) percentage of overthreshold time* (%)	95.6 (86.2)	36.9 (18.1)	25.9 (11.7)	2.1 (1.5)
Mean kV-on per track† (*n*)	—	7	15	13.4
Mean checkpoint updates (repositioning) per track† (*n*)	—	0.16	0.23	0.49

Abbreviation: kV = kilovoltage.
Proposed method yielded better targeting efficiency.
* Numbers were obtained from 74 three-dimensional tracks that contained overthreshold motion.
† Numbers were obtained by averaging all 536 three-dimensional tracks.

arc therapy. Compared with no motion monitoring, the data in Table 1 show that the periodic MV-kV scheme reduced the percentage of overthreshold time, leading to improved beam targeting. The targeting performance was improved if kV imaging was used more frequently (kV-on every 22.5° vs. kV-on every 45°). Compared with the periodic (every 22.5°) MV-kV method, the proposed method significantly reduced the overthreshold time for a similar amount of average kV use. No track had a percentage of overthreshold time of >2.1% using the proposed method. In contrast, the corresponding value was as great as 25.9% for the periodic (every 22.5°) kV imaging scheme. The total number of checkpoint updates was doubled for the proposed method. Together with better timing in the checkpoint updates, this explains why the percentage of overthreshold time was significantly reduced. The histograms of the percentage of overthreshold time, a good indicator of the motion monitoring efficiency, are shown in Fig. 7 for periodic kV imaging and the proposed protocols for the 74 tracks that contained overthreshold motion. The non-zero percentage of overthreshold time of the proposed method was attributed to the missed or delayed detection of overthreshold motion resulting from the small, but finite, probability of underestimating the marker displacement. These histograms further demonstrate the advantage of the proposed method in minimizing the percentage of overthreshold displacement.

DISCUSSION

A necessary step in combating the adverse effects of intrafraction prostate motion is real-time monitoring of the target position. Several methods for obtaining the data in real time have been proposed (10–12). Prostate tracking using electromagnetic transponders has recently been developed. However, in addition to its large physical size, the transponder produces severe magnetic resonance imaging artifacts and hinders magnetic resonance-based post-treatment assessments. Currently, x-ray imaging with implanted metallic fiducial markers remains the most reliable method to monitor organ motion.

Prostate motion tends to be random, without a fixed pattern (3, 13). A survey of previous studies indicated that, within an interval of 2 min, prostate motion >3 mm is present in ~5% of the observations. This increased to ~12% and ~25% at 5 and 10 min, respectively (5). These results suggest that intrafraction prostate motion during arc therapy is important, even though volumetric modulated arc therapy (VMAT) delivery takes less time than fixed-gantry intensity-modulated radiotherapy. Conservatively, after the initial patient setup, a RapidArc or VMAT session takes 2–5 min for 2-Gy/fraction deliveries. With increased interest in hypofractionated treatment and the use of multiple arcs (14), which protract the delivery, the need for intrafraction motion

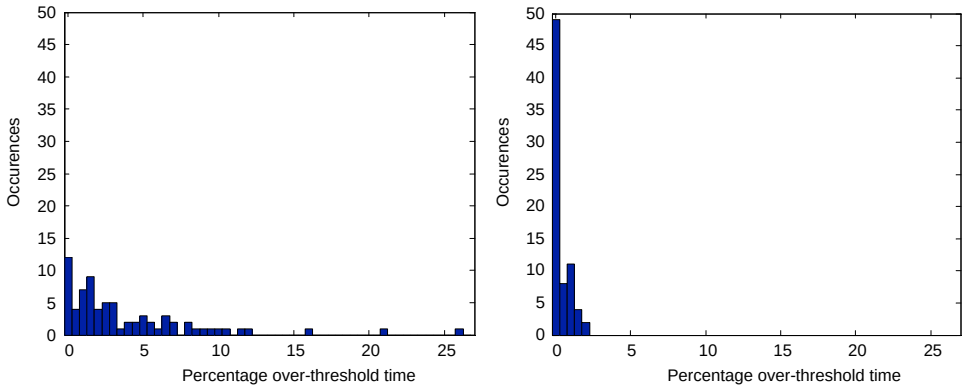

Fig. 7. Histograms of percentage of time of overthreshold displacements for periodic (every 22.5°) kilovoltage-on scheme (Left) and proposed method (Right).

monitoring during arc therapy will be increased further. Moreover, to document and verify the target position during arc therapy delivery, real-time monitoring of the prostate position will be important.

A conventional prostate motion monitoring strategy seeks to accurately and continuously localize the markers using fluoroscopic kV imaging. In contrast, a scheme similar to the ''failure detection'' strategy widely used in industrial engineering, in which a continuous accurate monitoring of system is not pursued until a warning signal from a failure detection device is triggered, has been proposed for prostate image-guided radiotherapy. Practically, it is neither necessary nor dose efficient to use continuous or periodic fluoroscopic kV imaging, together with the MV beam, because the prostate motion does not occur continuously. Thus, a kV-on signal is triggered only when the motion is greater than a specific threshold. Compared with other continuous kV-tracking modalities, which have generally required frequent use of kV beams, this technique offers sufficiently accurate target monitoring with a reduced imaging dose to the patient because the treatment is delivered in an arc. The scheme uses the treatment beam for ''failure detection'' and individualizes the use of kV imaging to each treatment session. On confirmation of an overthreshold displacement, a number of interventional strategies can be implemented to compensate for the motion (*e.g.,* moving the couch or shifting the subsequent MLC apertures; subjects of future research). The proposed approach is also suitable for monitoring other organs with slow and unpredictable motion.

The position estimation in the present study was done using MV projection pairs of $\sim 10^{\circ}$ apart. More sophisticated estimation of fiducial displacement with the optimal use of multiple MV projections at different times and other previous knowledge of prostate motion can be developed. Although this would be useful and might yield more accurate results, we do not anticipate any significant changes when multiple projection data are used for reconstruction.

When an intensity-modulated beam is used for in-line imaging, a potential difficulty is that the fiducial markers might be partially or completely blocked by the MLC leaves at certain angles. A fiducial blockage avoidance strategy has recently been studied in the context of intensity-modulated radiotherapy (15). It was shown that it is possible to ensure ''seeing'' at least one of the implanted fiducial markers in any of the intensity-modulated radiotherapy segments for monitoring the fiducials during a step-and-shoot dose delivery by adding to the objective function a hard or soft constraint that characterizes the level of preference for the fiducial marker to be included in the segmented fields. The final dose distributions of three plans (*i.e.,* constraint-free and soft and hard constraints) were very similar, which was understandable because the fiducial markers are generally placed inside the target volume, or prostate in the context of the present study. The strategy could be implemented for VMAT in a similar fashion. The combined gantry, marker, and MLC motion during VMAT, however, increases the problem complexity and the possibility of detection confusion among the markers. More efficient use of the information from the neighboring frames and incorporating speed constraints might alleviate this problem. Nevertheless, because three or four markers are usually used during treatment, the probability of detecting at least one marker is high, even with current RapidArc planning. Also, several sources of information that could help estimate the coordinates of an MLC-blocked fiducial marker were discussed in a previous report (7).

Although a relatively large marker was used in our experiments, segmentation of a clinically used gold marker can be achieved in real time with relatively high accuracy from simultaneously acquired MV and kV images of a pelvic phantom (16). Therefore, we do not foresee any major performance degradation in our ongoing clinical studies, which will be reported later.

CONCLUSION

A novel prostate motion tracking algorithm using cine-MV and as-needed kV imaging has been described. A distinct feature of the method is that continuous accurate position information is not actively pursued during the delivery process. Instead, the technique focuses its attention to detecting any motion potentially greater than a preset threshold (*i.e.,* ''failure'' detection) by taking advantage of the continuous gantry rotation during arc delivery. If motion occurs, kV imaging is triggered to accurately locate the current position of the prostate through triangulation with the MV data. The experimental and simulation data have shown that the proposed technique is capable of reliably tracking the prostate position during the arc therapy delivery process. It was able to provide high confidence about prostate displacement, without the unwanted overhead of continuous or periodic kV imaging. The technique can be readily implemented on linear accelerators equipped with electronic portal imaging device and onboard kV imaging devices.

REFERENCES

1. Kitamura K, Shirato H, Seppenwoolde Y, *et al*. Three-dimensional intrafractional movement of prostate measured during real-time tumor-tracking radiotherapy in supine and prone treatment positions. *Int J Radiat Oncol Biol Phys* 2002;53: 1117–1123.
2. Kotte ANTJ, Hofman P, Lagendijk JJW, *et al*. Intrafraction motion of the prostate during external-beam radiation therapy: Analysis of 427 patients with implanted fiducial markers. *Int J Radiat Oncol Biol Phys* 2007;69:419–425.
3. Kupelian P, Willoughby T, Mahadevan A, *et al*. Multi-institutional clinical experience with the Calypso System in localization and continuous, real-time monitoring of the prostate gland during external radiotherapy. *Int J Radiat Oncol Biol Phys* 2007;67:1088–1098.

4. Malinowski KT, Noel C, Roy M, *et al*. Efficient use of continuous, real-time prostate localization. *Phys Med Biol* 2008;53: 4959–4970.
5. Langen KM, Willoughby TR, Meeks SL, *et al*. Observations on real-time prostate gland motion using electromagnetic tracking. *Int J Radiat Oncol Biol Phys* 2008;71:1084–1090.
6. Li HS, Chetty IJ, Enke CA, *et al*. Dosimetric consequences of intrafraction prostate motion. *Int J Radiat Oncol Biol Phys* 2008;71:801–812.
7. Liu W, Wiersma RD, Mao W, *et al*. Real-time 3D internal marker tracking during arc radiotherapy by the use of combined MV-kV imaging. *Phys Med Biol* 2008;53:7197–7213.
8. Wiersma RD, Mao WH, Xing L. Combined kV and MV imaging for real-time tracking of implanted fiducial markers. *Med Phys* 2008;35:1191–1198.
9. Murphy MJ, Balter J, Balter S, *et al*. The management of imaging dose during image-guided radiotherapy: Report of the AAPM Task Group 75. *Med Phys* 2007;34:4041–4063.
10. Adamson J, Wu Q. Optimizing monoscopic kV fluoro acquisition for prostate intrafraction motion evaluation. *Phys Med Biol* 2009;54:117–133.
11. Balter JM, Wright JN, Newell LJ, *et al*. Accuracy of a wireless localization system for radiotherapy. *Int J Radiat Oncol Biol Phys* 2005;61:933–937.
12. Poulsen PR, Cho B, Langen K, *et al*. Three-dimensional prostate position estimation with a single x-ray imager utilizing the spatial probability density. *Phys Med Biol* 2008;53:4331–4353.
13. Kupelian PA, Langen KM, Willoughby TR, *et al*. Image-guided radiotherapy for localized prostate cancer: Treating a moving target. *Semin Radiat Oncol* 2008;18:58–66.
14. Bortfeld T, Webb S. Single-Arc IMRT? *Phys Med Biol* 2009; 54:N9–N20.
15. Ma Y, Lee L, Keshet O, *et al*. Four-dimensional inverse treatment planning with inclusion of implanted fiducials in IMRT segmented fields. *Med Phys* 2009;36:2215–2221.
16. Mao W, Riaz N, Lee L, *et al*. A fiducial detection algorithm for real-time image guided IMRT based on simultaneous MV and kV imaging. *Med Phys* 2008;35:3554–3564.

Learning Objectives:
1. Describe ways in which molecular imaging can help direct cancer therapy.
2. Discuss the complementary role of in vitro assay and in vivo imaging in measuring cancer phenotype.
3. List examples of how imaging can be used to help direct cancer therapy.

TU-C-BRC-02

Infrastructure to Integrate Imaging in Clinical Trials

D Sullivan[1] *, (1) , Duke University Medical Center

Imaging biomarkers are increasingly used as primary or secondary endpoints in therapeutic trials. There are many academic units, professional organizations, industry groups and federal agencies addressing one or more components or issues associated with imaging biomarkers, and communication and coordination of efforts has been minimal. The RSNA has organized an Imaging Biomarkers Roundtable to establish ongoing communication among these organizations, and to develop a roadmap of activities and goals.

Validation of imaging methods as biomarkers is complicated by the variability within and between patients, by the human observer component, by the variability across imaging devices from different manufacturers, and by the need to standardize methods across institutions and centers. To understand the errors and reduce them where possible, the Quantitative Imaging Biomarkers Alliance (QIBA) has been formed. These and other efforts are active and productive. Accomplishments and future plans will be discussed.

Learning Objectives:
1. Understand efforts to integrate imaging biomarkers in clinical trials.
2. Understand efforts to improve the accuracy and precision of imaging biomarkers.

TU-C-BRC-03

AAPM Initiatives in Quantitative Imaging

JM Boone[1] *, (1) UC Davis Medical Center, Sacramento, CA

The Science Council (SC) of the AAPM has initiated the Quantitative Imaging (QI) Initiative, which is an effort focused on moving the field of diagnostic imaging towards a more quantitative footing. While much of the quantitative content of the radiologist report will be generated by the radiologist with perhaps the help of user-friendly and robust software capable of generating quantitative metrics off of a patient's images, there is an important role for physicists to play in assuring the quantitative integrity of the image data. The QI Initiative currently has three task groups, on PET/CT, on dynamic contrast enhanced MRI, and on CT. The methods and activity of these groups towards achieving their objectives will be discussed. The activity of these three groups has overlap with similar efforts of other societies such as the SNM, ISMRM, and the RSNA, and the interconnections will also be described. The parallel, integrated efforts towards creating a more quantitative future for medical imaging assessment is being driven by the needs of clinical research trials, as well as other payer initiatives such as pay for performance. Long term, the QI Initiative will include a comprehensive array of procedures to reduce variance in the imaging process, by standardization of the acquisition protocols, calibration of the spatial and gray scale output of scanners, incorporation of structured reporting tools to improve accuracy and format consistency, and the development of scientific software capable of extracting accurate QI data from image data.

Joint Imaging/Therapy Scientific Session
Room 303A
Modeling of Intrafraction Motion

TU-C-303A-01

Evaluating the Accuracy of Four-Dimensional Photon Dose Calculations with Phantom Measurements

Y Vinogradskiy*, P Balter, D Followill, P Alvarez, A White, G Starkschall, UT MD Anderson Cancer Center, Houston, TX

Purpose: Respiratory motion can cause deviations between the intended and delivered dose distributions. Recent work has focused on developing four-dimensional (4D) dose calculation algorithms, which explicitly account for respiration in the dose calculation process. Before these dose calculations methods can be used clinically, it is necessary to verify their accuracy. The purpose of this study was to evaluate the accuracy of 4D dose calculations with phantom measurements. **Methods**: Measurements were made using two anthropomorphic phantoms: a rigid moving phantom and a deformable phantom. Two motion patterns were designed to drive both phantoms: a sinusoidal motion pattern and an irregular motion pattern that was extracted from a patient breathing profile. Three plans were generated on each phantom: a single-beam, a multiple-beam, and an IMRT plan. Doses were calculated using the 4D dose calculation capabilities of a commercial radiation treatment planning system. Each plan was used to irradiate the phantoms, and doses were measured using TLD and radiochromic film. The measured doses were compared to the 4D-calculated doses using a measured-to-calculated TLD ratio and a gamma analysis. For the TLD and film, relevant passing criteria (5% for TLD and 5%/3mm for gamma) were applied to determine if the 4D dose calculations were accurate to within clinically acceptable standards.
Results: All of the TLD measurements met the passing criteria. 42 out of the 48 evaluated films passed the gamma criteria. The films that did not pass the gamma criteria were from the irregular moving rigid phantom.
Conclusions: In controlled conditions, 4D dose calculations are accurate to within clinically acceptable standards. In clinical terms, this means that if patient breathing is reproducible, 4D dose calculations will produce accurate dose distributions. Conversely, irregular breathing can produce inaccurately calculated 4D dose distributions. **Conflict of Interest:** This work is partially supported through an SRA with Philips Healthcare.

TU-C-303A-02

Intrafraction Prostate Motion Monitoring with Cine-MV and Minimal As-Needed Onboard KV Imaging

W Liu[1] *, Y Xie[2] , G Luxton[1] , R Wiersma[3] , L Xing[1] , (1) Stanford University School of Medicine, Stanford, CA, (2) Peking University, Beijing, Beijing, CN, (3) The University of Chicago, Chicago, IL

Purpose: To examine the feasibility and performance of using treatment MV beam imaging with prior knowledge to estimate 3D prostate intrafraction motion and to instantaneously reposition based on information from minimal usage of on-board kV imaging during IMRT. **Methods and Materials:** In contrast with current motion monitoring techniques which seek to accurately and continuously localize a moving target, we attempted for the first step only to detect potential motion beyond a pre-defined threshold using MV images and in the second step through combined MV-kV imaging (by turning on the kV imager) to confirm the over-threshold event as well as obtaining accurate position information which could be used for instantaneously repositioning. EPID images were used to measure 2D prostate displacement in the imaging plane. By taking into account the strong correlation between prostate SI and AP motion, small displacement in the LR direction, and data from a previous IMRT session (different gantry angle), we estimated in-line prostate motion as well which in turn allowed us to detect potential 3D over-threshold motion. To minimize the influence from training data, no statistical motion probability distribution information was used. Simulation has been done using 536 patient-measured trajectories from 17 patients. Experiments were performed on a Varian Trilogy linac using a motion phantom programmed for selected typical trajectories, and the results were compared with simulations. **Results:** Prostate displacement beyond a set threshold (3mm) was detected for over 99% of the time at the cost of negligible kV dose (< 3 images/fraction on average). The position information required for repositioning was found to have sub-millimeter accuracy using combined MV-kV data. **Conclusion:** Significant reduction of adverse effects of intrafraction prostate motion is achievable. The technique can be readily implemented in clinics and incurs minimal imaging dose to the patient as compared with other stereoscopic imaging techniques.

TU-C-303A-03

Real-Time Profiling of Respiratory Motion and Its Application to Continuous Horizon Prediction

D Ruan[1] *, J Fessler[2] , J Balter[2] , P Keall[1] , (1) Stanford University Cancer Center, Stanford , CA, (2) The University of Michigan, Ann Arbor, MI

Purpose: Respiration-induced tumor motions are semi-periodic and exhibit different variations that have distinct clinical implications. We

The techniques developed for the commissioning also provided reliable methods for future system quality assurance.

TH-C-BRC-10

Evaluation of a Micro-CT Based 3D Conformal Animal Radiotherapy System

H Zhou[1] *, J Xu[2] , M Rodriguez[3] , F van den Haak[1] , X Zhu[2] , Y Xian[4] , G Nelson[1] , R Jogani[1] , P Keall[1] , E Graves[1] , (1) Stanford University, Stanford, CA, (2) PheniCo Inc., Fremont, CA, (3) Universidad Nacional Autonoma de Honduras, Tegucigalpa, Honduras (4) Bright Star Machine, Fremont, CA

Purpose: To treat small animal disease models with clinically-relevant radiotherapy strategies, an image-guided 3D conformal radiotherapy system based on a microCT imaging device has been constructed. **Method and Materials:** A variable-aperture collimator was installed in a GE RS120 microCT, so that the beam width could be adjusted between 0 to 100 mm at the CT isocenter. The collimator was aligned with the X-ray beam axis through film and detector measurements. A two-dimensional translation stage was integrated with the existing z-stage of the scanner to allow 3D positioning of a subject within the CT bore. Radiation treatment planning software is based on the RT_Image application, including tools to specify treatment parameters based on the CT image and an EGSnrc-based Monte Carlo dose calculation package. To test this system, two mice with spontaneous lung tumors have been irradiated to a dose of 2 Gy. **Results:** Automation of the system has been realized through high-precision mechanical design and assembling of the collimator and stage, the calibration, and the control software. Geometric and dosimetric calibration of the system has resulted in beam width and position precisions better than 0.1 mm, and dose precision better than 3%. The treatment planning software development can specify treatment parameters within the coordinate frame of the CT image, which can then be used to control the device hardware. Mice with lung tumors were irradiated with the system. Post-mortem immunohistochemical assays demonstrated the presence of DNA double strand breaks within the radiation target. **Conclusion:** We have demonstrated the accuracy and utility of a novel microCT-based image-guided 3D conformal radiotherapy system. Clinically-similar image-guided radiation therapy has been applied to small animals, facilitating future investigations of this technology in the laboratory.

Joint Imaging/Therapy Scientific Session
Room 303A
Target Localization

TH-C-303A-01

Initial Clinical Experience with Electromagnetic Localization and Tracking for External Beam Partial Breast Irradiation

M K N Afghan *, S Eulau , A Morris , P Hallam , J Ye , T Wong , D Cao , T Zeller , T Mate , D Shepard , Swedish Cancer Institute, Seattle, WA

Purpose: The Calypso® 4D Localization System™ (Calypso Medical) uses non-ionizing AC electromagnetic radiation to localize and track small wireless devices (called Beacon® transponders) implanted in or near a patient's tumor. We report on the first clinical experience with the use of the system for localizing and tracking the lumpectomy cavity during external-beam accelerated partial breast irradiation (EB APBI). **Method and Materials:** The study included patients treated receiving EB APBI on an IRB approved protocol. Thirteen patients were implanted with both gold markers (GM) and beacon® transponders and two patients were implanted with beacon® tranponders alone. For patients in whom MRI follow-up was anticipated, two removable interstitial breast catheters were inserted and afterloaded with gold markers and transponders. The catheters were removed post radiation therapy. Initial alignment was performed using lasers. For patients with gold markers, orthogonal images were used to obtain the necessary shift. The shift values were compared to the shift predicted under electromagnetic guidance. During treatment, Calypso was used to track the target motion. **Results:** Fifteen patients have been studied, and 93 treatment fractions were analyzed. The catheters and transponders overall showed good stability with inter-transponder distance changes of less than 2 mm. Calypso based setup can be performed in less than 2 minutes. An average residual setup error of 10.29 mm was determined using gold markers. For the 63 fractions analyzed, the difference between the residual setup error determined by the GM and the Calypso system on average was 1.5 mm. Tracking showed regular motion in the range of 2-3 mm with occasional deeper breaths exceeding 4-5 mm. **Conclusion:** Results show excellent agreement between gold markers and electromagnetic guidance in EB APBI with electromagnetic guidance providing a more rapid setup and real time tracking during delivery.

Research sponsored by Calypso Medical.

TH-C-303A-02

Clinical Data Evaluation of Fiducial-Free Spine Tracking for CyberKnife Radiosurgery

D Fu* , H Zhang , H Wang , B Wang , G Kuduvalli , CR Maurer Jr, Accuray Incorporated, Sunnyvale, CA

Purpose: To evaluate the accuracy of the Xsight® Spine Tracking (XST) System in the CyberKnife® Robotic Radiosurgery System (Accuray Incorporated, Sunnyvale, CA) using retrospective analysis of clinical data. **Method and Materials:** The XST System performs patient alignment and frequent intra-fractional tracking for spine radiosurgery. The 3 translations and 3 rotations of the 3D transformation are computed and used for treatment couch correction in patient setup and radiation beam position compensation during treatment delivery. The XST System eliminates the need for fiducials by using 2D-3D spine registration of two orthogonal X-ray images and the planning CT image. Analysis was performed using image data acquired for 26 patients previously treated using fiducial tracking. The data consists of a CT image for each patient plus 4,480 X-ray image pairs acquired during treatment. The cases cover the entire spinal column (3 cervical, 13 thoracic, 7 lumbar and 3 sacrum). Each patient had 4–6 metal fiducials implanted in vertebrae adjacent to the spine lesion being treated. Fiducial and XST tracking were performed for all X-ray image pairs. The XST transformation errors were calculated by using the fiducial tracking results as the reference gold standard. **Results:** The error of each translation component is <0.5 mm in 20/26 patients, <1 mm in 25/26 and <1.5 mm in 26/26. The mean 3D translation error is 0.6 mm. The error of each rotation component is <0.5° in 9/26, <1° in 23/26, <1.5° in 25/26 and <2° in 26/26. The mean total rotation error is 0.8°. For 1 patient with >1 mm translation error and 3 patients with >1° rotation error, the fiducials are far from the center of region of interest, which degrades the fiducial tracking accuracy. **Conclusion:** The XST System robustly tracks all spine regions and accurately computes both translations and rotations.

Research sponsored by Accuray Incorporated.

TH-C-303A-03

Real-Time Motion Detection of Prostate Target During Volumetric Arc Therapy Using Onboard Imaging Devices

W Liu[1] *, R Wiersma[2] , G Luxton[1] , L Xing[1] , (1) Stanford University School of Medicine, Stanford, CA, (2) The University of Chicago, Chicago, IL

Purpose: To develop a real-time prostate position monitoring technique for modern arc radiation therapy through novel usage of cine-MV imaging together with as-needed kV imaging. **Methods and Materials:** We divide the task of monitoring intrafraction prostate motion into two separate but related parts: (1) to detect potential target motion beyond a pre-defined threshold and (2) to confirm whether it is beyond the threshold and how large the displacement is. By taking advantage of the gantry rotation during arc therapy, MV images from different viewing angles were used to stereoscopically evaluate the motion status of the prostate/marker and to allow us to detect potential over-threshold displacement. If a potential over-threshold event is detected by MV images, the onboard kV imager is turned on to confirm this through combined data from MV-kV imaging. The position information acquired from combined MV-kV data can be used as input for further motion management techniques. A Varian Trilogy linac with onboard kV imager was used to examine selected typical trajectories using a 4D motion phantom capable of moving in accordance with a pre-programmed trajectory. Performance analysis of the proposed method has been done using 536 patient-measured trajectories from 17 patients. **Results:** Prostate displacement beyond a set threshold (3mm) was detected for over 99.8% of the time with better than 1mm detection accuracy. Compared to other fluoroscopy-based tracking techniques, kV usage is significantly reduced to on average of ~15 times per arc delivery. **Conclusions:** Cine MV imaging during arc therapy provides a valuable

tool for detecting non-negligible intrafraction prostate motion with as-needed low kV usage. Our motion detection method is distinguished from current motion monitoring techniques which seek to continuously and accurately localize a moving target. The proposed technique can be readily implemented with linacs equipped with EPID and onboard kV imaging devices.

TH-C-303A-04

Evaluation of 3D Surface Camera System in Patient Setup for HN RT

O Gopan[1, 2] *, Q Wu[3, 4] , (1) William Beaumont Hospital, Royal Oak, MI, (2) Wayne State University, Detroit, MI, (3)Duke University Medical Center, Durham, NC, (4) William Beaumont Hospital, Royal Oak, MI

Purpose: To evaluate the usefulness of a 3D surface camera system (AlignRT) in detecting rigid and non-rigid setup errors during head and neck radiotherapy. **Methods and Materials:** To evaluate the accuracy of AlignRT's surface registration algorithm, both translational and rotational movements of a known magnitude were manually applied in Pinnacle to transform a helical CT scan. The skin contours of both the primary helical CT scan and the transformed helical CT scan were transferred to AlignRT, where the transformed surface was registered to the primary surface. The changes that were reported by the AlignRT system were compared to the manually applied motions from Pinnacle. To evaluate the usefulness of AlignRT for rigid and non-rigid patient setup, a retrospective analysis was performed on the helical CT scans of eleven patients. The registrations in Pinnacle based on bony (either skull (rigid) or vertebrae (non-rigid)) anatomy were compared to the surface (either head (rigid) or shoulder (non-rigid)) registrations in AlignRT. **Results:** The accuracy of AlignRT's surface registration algorithm was, on average, 0.041 ± 0.036 degrees and 0.075 ± 0.100 mm. The accuracy of the optical system was, on average, 0.087 ± 0.912 degrees and -0.153 ± 1.996 mm. For shoulder (non-rigid) guidance, if we use 2*standard deviation for 95% confidence level, the accuracy of the optical system was within 3 degrees for rotations in the vertical and longitudinal directions, but 5 degrees for the lateral direction. For translations, the accuracy was more than 10 mm.
Conclusion: While the feasibility of using the AlignRT system for head (rigid) guidance in the setup of HN patients was demonstrated, the use of the system in non-rigid patient setup yielded undesirable results.

TH-C-303A-05

Development of a Dynamic KV Collimator for Low Diagnostic Dose Real-Time 3D Motion Tracking During Radiation Therapy by Combined MV-KV Imaging

R Wiersma[1] *, E Pearson[1] , C Pelizzari[1] , (1) The University of Chicago, Chicago, IL

Purpose: Currently, real-time 3D MV-kV monitoring requires the use of continuous kV imaging throughout the treatment process leading to high diagnostic dose costs. For MV-kV tracking purposes the only needed kV image information are the projected images of the metallic fiducial markers. Generally these markers are small (3mm in length and 0.8mm in diameter), and for a standard 40cm x 30cm kV image comprise less than 1% of the total area. The proposed technique here uses a dynamic kV aperture to confine the kV exposure to a small region of interest (ROI) encompassing only the markers. As the internal markers move, the aperture is dynamically updated using feedback information provided by the last known marker positions. **Method:** A Varian Trilogy equipped with both an EPID and a kV imaging system was used. The kV collimator was mounted over the kV source and consists of four lead blades placed orthogonally on low friction linear guide rails. The position of each blade was controlled independently using a servomotor. MV-kV imaging was performed and software was used to calculate a suitable ROI that will be used as an input for the kV collimator. As the internal markers move, the aperture will be dynamically updated using the last known marker positions. **Results:** The combination of controller circuitry and chosen servomotors allows for blade travel speed of up to 11mm/s, depending on orientation, with an accuracy of 0.2mm in the collimator plane. This should be sufficient to keep the ROI properly centered on nearly any fiducial cluster. **Conclusion:** The technique proposed here would potentially lower the kV exposure by a factor of 50–500 depending on the speed, number, and spatial separation of the fiducials. The technology is directly applicable to any kV imaging system where only selective ROI information is required.

TH-C-303A-06

Performance Characterization of a MVCT Scanner Using Multi-Slice Thick, Segmented Cadmium Tungstate-Photodiode Detectors

P Kirvan , S Rathee *, T Monajemi , B Fallone , Cross Cancer Institute, Edmonton, AB, CA

Purpose: To evaluate the performance of a MVCT system based on multi-slice, thick, and segmented cadmium tungstate-photodiode detectors. **Method and Materials**: Our MVCT's detector is a 2D array of 1mm x 1mm (pitch) x 10mm (thickness) cadmium tungstate crystals separated by a septa paint of reflectivity higher than 0.975. The scintillators are mounted on ten 16 x 16 element photodiode arrays (SCA-CA256ES, Semicoa, Costa Mesa, CA). The total array size is 320 detectors along the arc by 16 detectors along the slice thickness direction. The radius of curvature of detector arc is 92.5cm. In our system, the source and detectors remain stationary while the object being imaged is placed on a precision rotating stage. Due to the high dose per pulse provided by our clinical linac, it is not possible to image a test object with a dose of < 50cGy in a 6MV beam. In order to obtain low dose images, we used the small amount of Bremsstrahlung radiation produced in the scattering foils in 6 MeV electron beam after removing the electrons from the beam by placing 4cm of solid water in the beam. **Results**: Our system demonstrates a uniformity index of 0.4% at 1.9cGy. The noise standard deviation is around 2% at 1.9cGy. CT number linearity (R^2= 0.9982) and low contrast resolution (15 mm object with 1.5% contrast at 2 cGy) are superior to published evaluations of commercially available tomotherapy MVCT. The spatial resolution is about 4lp/cm which is limited mainly by the diffused Bremsstrahlung source. **Conclusion**: Thick segmented cadmium tungstate detectors offer significantly better low contrast resolution per unit dose at MV energy than commercially available gas filled or flat panel detectors. This work demonstrates the feasibility of creating a fully functional MVCT system using this technology.

TH-C-303A-07

A Diaphragm Tracking Algorithm for Megavoltage Cone Beam CT Projection Data

M Chen*, R Siochi, University Of Iowa, Iowa City, IA

Purpose: To test a novel algorithm for diaphragm detection in 2D views of cone-beam computed tomography (CBCT) raw data. **Method and Materials:** 6 Siemens megavoltage CBCT scans of lungs were analyzed. For each scan, a user identified the diaphragm apex in two full exhale and two full inhale views to determine exhale and inhale bounding points, respectively, in room coordinates. Projecting bounding points into other views creates opposite corners of a bounding rectangle that is enlarged to create a cost function region (CFR). A cost image is created by multiplying the gradients of the Gaussian filtered CFR with a gradient direction matching function, based on diaphragm contour training sets. The sum of cost image values along a parabolic path is V(a, x_0, y_0, t), where the parameter set (a, x_0, y_0, t) describes a parabola whose vertex is constrained within the bounding rectangle of the view at index t. Dynamic programming finds the path in this 4D parameter space that maximizes the sum of V, over all views, subject to smoothness constraints between adjacent views. The results were compared to the expert-identified diaphragm apex. Errors were calculated in room coordinates as the root-mean-square distances between the expert's points and the parabola's vertices in all 200 views. Room coordinates were calculated by interpolated ray-tracing. **Results:** The diaphragm was successfully detected in all 6 data sets, even for views with poor image quality and confounding objects. Each CBCT scan analysis (200 views) took about 35 seconds on a 2.66 GHz Intel quad-core 2 CPU. The average cranio-caudal position error was 1.58 ± 0.44 mm. Other directions were not assessed due to uncertainties in expert identification, so future studies will use anthropomorphic motion phantoms. **Conclusion:** The diaphragm detection algorithm is sufficiently quick and accurate for motion determination prior to radiation therapy.

Author Disclosure: M. Takagi, None; K. Sakata, None; M. Someya, None; H. Tauch, None; Y. Matsumoto, None; T. Torigoe, None; A. Takahashi, None; M. Hareyama, None; M. Fukushima, None.

2866 The Radiosensitizing Effects of Titanium-dioxide Nanoparticles *In Vitro*

J. M. Boyle, A. Wu, H. Arora, T. Paunesku, G. E. Woloschak

Northwestern University, Chicago, IL

Purpose/Objectives: Our laboratory investigates different potential uses of TiO_2 nanoparticles as vehicles for bio-nanotechnology. Nanoconjugates have been designed which consist of a nanoparticle covalently bound to nucleic acid sequences which allow targeting of the nanoconjugates to oncogenes with sequence specificity. Subsequent exposure to photons at 3.2 eV or greater takes advantage of the photocatalytic properties of TiO_2 and allows for sequence specific DNA cleavage. Past studies have used UV xenon lamp irradiation to induce cleavage. Due to the limited tissue penetration of UV visible light, the utility of the nanoconjugates is limited to superficial in vivo targets. The goal of current experiments was to investigate the potential to excite of TiO_2 nanopartivlesnanoparticles to be excited with ionizing gamma radiation, which would extend extending their utility to internal in vivo targets. The endpoint for the experiment described here was cell killing of cultured cells.

Materials/Methods: 8 nm nanoparticles (NPs) made of cobalt-iron oxide with titanium-dioxide shell were synthesized and dialyzed against 10mM Na_2HPO_4 buffer (pH=7). HeLa cells in culture at 90% confluency were serum starved and exposed for four hours to (a) 200 nM NPs at 200 nM in media; (b) 5 Gy of gamma radiation; (c) 200 nM NP at 200 nM in media followed by ionizing radiation (5 Gy) or (d) nothing. Following treatment, cells were left in media for one day to allow for cell death to occur. To determine dead cell numbers, DAPI stain was used and cells were submitted for to FACS analysis, and data quantification was done using FCS Express software.

Results: Cells pretreated with NPs and 5 Gy of ionizing radiation resulted in showed an increase in cell mortality as compared to treatment with NPs or radiation alone. Cells treated with NPs alone did show higher rates of mortality than in non-treated control cells with no treatment. Results of three trials comparing cells treated with NPs and radiation vs. radiation alone showed rates of mortality of 33.610% vs. 15.947% (p=0.0385).

Conclusions: Pre-treatment of cells with NPs increased the cytoxic effect of subsequent treatment ionizing radiation. Comparison of equal doses of radiation in cells pre-treated with NPs and with no pre-treatment showed that NPs increased the cytotoxic effect of radiation by 111%. Current studies are underway to both find the treatment conditions that maximize the observed cytotoxicity and to determine mechanisms of cytotoxicity underlying it.

Author Disclosure: J.M. Boyle, None; A. Wu, None; H. Arora, None; T. Paunesku, None; G.E. Woloschak, None.

2867 Chemotherapy can Enhance the Therapeutic Potential of Vaccine-mediated Immunotherapy

J. A. Caballero[1], S. Gameiro[1], J. Higgins[1], A. Boehm[1], A. Franzusoff[2], J. Schlom[1], J. Hodge[1]

[1]*Laboratory of Tumor Immunology and Biology, Center for Cancer Research, National Cancer Institute, National Institutes of Health, Bethesda, MD,* [2]*GlobeImmune, Inc., Louisville, CO*

Purpose/Objective(s): Previous studies have shown that chemotherapy given prior to vaccine can inhibit vaccine mediated antitumor immunity. Since chemotherapy is standard of care for many cancer types, the possibility that chemotherapy can be used concomitantly with vaccine was evaluated. We hypothesized that one could take advantage of the fact that certain chemotherapy regimens induce transient pancytopenia, which is followed by a recovery phase. We examined if administering vaccine during the T-cell recovery phase would enhance the effectiveness of the vaccine. Moreover, we examined the effects of chemotherapy on the quantity and function of regulatory T-cells. Many non-small cell lung cancer (NSCLC) patients undergo surgery followed by standard-of-care adjuvant chemotherapy, which includes cisplatin in combination with vinorelbine. In spite of therapy, the median survival of patients with metastatic disease is less than 10 months.

Materials/Methods: We evaluated the potential for biological synergism between the standard-of-care chemotherapy regimen and a recombinant yeast-CEA vaccine in a mouse model of NSCLC. We also examined the translational potential of our preclinical findings by evaluating the effect of chemotherapy on CTL-mediated cytolysis of human NSCLC tumor cell lines in vitro.

Results: These studies demonstrate for the first time that (a) the combination of cisplatin plus vinorelbine modulates CD4+, CD8+, CD19+, natural killer, and regulatory T-cell populations in healthy mice; and (b) cisplatin plus vinorelbine combined with heat-killed recombinant yeast-CEA vaccine (i) is superior to either modality alone at reducing tumor burden and (ii) increases vaccine mediated antigen-specific T-cell responses. Moreover, cisplatin plus vinorelbine modulates the cell surface expression of immunologically relevant molecules and improves antigen-specific CTL mediate cytotoxicity in vitro.

Conclusions: These finding suggest potential clinical benefit for the combined use of recombinant yeast vaccine and cisplatin-based chemotherapy regimens.

Author Disclosure: J.A. Caballero, None; S. Gameiro, None; J. Higgins, None; A. Boehm, None; A. Franzusoff, Vice President and Scientific Founder, GlobeImmune, Inc., A. Employment; J. Schlom, None; J. Hodge, None.

2868 Optimized Hybrid MV-kV Imaging Protocol for Volumetric Prostate Arc Therapy

W. Liu, G. Luxton, L. Xing

Stanford University School of Medicine, Stanford, CA

Purpose/Objective(s): Combined fluoroscopic kV and MV imaging has been shown to be capable of real-time 3D monitoring of tumor motion with sub-millimeter accuracy. For prostate arc therapy, however, it is neither necessary nor dose-efficient to use

continuous fluoroscopic kV imaging, because prostate motion occurs only sporadically during dose delivery. Here we develop a protocol for as-needed kV imaging triggered by prostate motion status derived from continuously-updated MV images during volumetric arc therapy.

Materials/Methods: In volumetric modulated arc therapy delivery, cine MV images are taken at different gantry angles. The sequential MV projections are utilized to examine whether fiducial positions have changed, and to stereoscopically detect potential displacements beyond a pre-defined threshold. In addition, we algorithmically take into account the fact that prostate SI and AP motions are strongly correlated and the prostate is more stable in LR direction. When a potential over-threshold displacement (3 mm in this work) is detected, the kV imager is turned on to determine the ''true'' fiducial position through simultaneous MV-kV imaging. Choice of threshold is empirical and determined by desired delivery accuracy and minimizing use of kV imaging. The scheme is similar to the ''failure detection'' strategy widely used in industrial engineering, where a continuous accurate monitoring of markers is not pursued until a warning signal from the failure detection device is triggered. A Varian Trilogy with an onboard kV imager was used to implement this prostate monitoring strategy during arc therapy. System calibration was used to compensate for geometric localization error from gantry sag and imager tilt. The performance of the prostate motion detection technique was evaluated using a 4D motion phantom programmed with 20 tracks of relevant patient prostate motions selected from 536 analyzed Calypso patient-measured trajectories.

Results: The usage of kV imaging was significantly reduced compared to the conventional combined MV-kV imaging scheme. It was found that on average, only 4 kV images per 2 Gy treatment fractions were needed to accurately detect over-threshold prostate motion, with 0.2% of time corresponding to prostate displacement greater than 3 mm not being detected.

Conclusions: An optimized hybrid MV-kV imaging strategy for prostate volumetric arc therapy has been validated. In contrast with the commonly used motion monitoring strategy which seeks to continuously localize a target, the proposed technique emphasizes detecting only clinically-relevant displacements, and intelligently switching on the kV beam. The proposed method provides real-time, clinically-needed, accurate prostate position information without the overhead of excessive imaging dose

Author Disclosure: W. Liu, None; G. Luxton, None; L. Xing, None.

2869 Potential Dose Escalation to Prostate Cancer using Electromagnetic Transponders: Effect of Margin Reduction on OAR and Treatment Time

D. Mah, C. Chen, E. Milan, S. Tsai, M. Garg, L. Hong, R. Yaparpalvi, S. Kalnicki

Montefiore Medical Center, Bronx, NY

Purpose/Objective(s): Implanted Calypso Beacon electromagnetic transponders (EMT) permit real time localization of the prostate. Knowledge of the prostate position using EMT permits margin reduction, but requires therapist intervention, thereby increasing treatment time. We investigate the feasibility of dose escalation using different PTV margins, and the trade off between margin reduction and increase in treatment time.

Materials/Methods: Treatment plans with GTV to PTV margins of 3 mm, 5 mm, and our standard 1 cm margin with 7 mm posterior expansion were evaluated for 9 prostate cancer patients undergoing 7 field sliding window IMRT (Eclipse, Varian) with EMT. Plans were generated for each patient with the goal of dose escalation to 86.4 Gy for each margin with 100% of the prescription covering 95% of the PTV. Rectal constraints included $V_{47Gy}<53\%$ and $V_{65Gy}<17\%$; bladder was constrained to $V_{47Gy}<53\%$ and $V_{65Gy}<25\%$. The 320 motion records for the 9 patients were retrospectively analyzed. The duration of each record was ~500 seconds. Drifts from the initial zero position beyond the margin triggered an intervention when they lasted more than the 3 second threshold. Each intervention (therapist entering the room to reposition the patient) is modeled as lasting 3 minutes.

Results: When planned with standard margins, all 9 patients were disqualified for dose escalation to 86.4 Gy. Seven patients were unable to meet the $V_{65Gy}< 17\%$ rectal constraint when planned with a 5 mm margin and five failed with a 3 mm margin. Two patients failed the $V_{47Gy}<53\%$ constraint with 5 mm margin and only one failed with a 3 mm margin. All bladder constraints for 5 and 3 mm margins were met. For standard, 5, and 3 mm margins, the mean intervention frequency per fraction, based on the motion records, was 0.04, 0.09 and 0.25, requiring a predicted total additional intervention time of 6, 13, and 36 minutes per patient over a 48 fraction course.

Conclusions: Dose escalation to prostate with margin reduction is ultimately limited by rectal constraints. Reduction of margin from our standard margin to 3 mm, enabled by accurate EMT, would facilitate dose escalation for 4 of 9 patients. Despite tight tracking limits, the frequency of interventions and efficiency of treatment is clinically manageable. One approach to reduce the intervention time would be to establish a remote couch correction.

Author Disclosure: D. Mah, Received software from Calypso Medical for this project, C. Other Research Support; C. Chen, None; E. Milan, None; S. Tsai, None; M. Garg, None; L. Hong, None; R. Yaparpalvi, None; S. Kalnicki, Calypso Medical, F. Consultant/Advisory Board.

2870 Prospective Study of Cone-beam CT (CBCT) Guidance for Prone Accelerated Partial Breast Irradiation (APBI)

G. Jozsef, S. C. Lymberis, K. J. DeWyngaert, S. C. Formenti

New York University Clinical Cancer Center, New York, NY

Purpose/Objective(s): An obvious risk of APBI is that it may result in a greater possibility of geographical miss. As part of NYU 07-582 we used CBCT to analyze and reduce setup errors of prone APBI.

Materials/Methods: Eligible to this IRB-approved protocol is post-menopausal women with pT1 breast cancer excised with negative margins without EIC and no axillary nodal involvement. Prone APBI consists of five 6 Gy daily fractions of image guided radiotherapy (Total dose=30 Gy). Patients are setup prone, on a dedicated mattress, used for both simulation and treatment. CBCTs are performed with Varian OBI kV imaging system (FOV 35 cm, slice thickness 2.5 mm) to enhance inter-fraction reproducibility of the setup after standard skin marks and laser alignment. CBCT images are registered to the planning CT and the resulting shifts